



## RESEARCH ARTICLE

10.1029/2025JH000667

## Key Points:

- Bayesian inference can identify sources for complicated inverse problems
- Estimates of the posterior Hessian provide uncertainty estimates
- Anecdotal historical records of tsunamis can provide meaningful seismic information

## Correspondence to:

J. P. Whitehead,  
[whitehead@mathematics.byu.edu](mailto:whitehead@mathematics.byu.edu)

## Citation:

Glatt-Holtz, N. E., Harris, R. A., Holbrook, A. J., Krometis, J., Kurniawan, Y., Ringer, H., & Whitehead, J. P. (2025). Embracing uncertainty in “small data” problems: Estimating earthquakes from historical anecdotes. *Journal of Geophysical Research: Machine Learning and Computation*, 2, e2025JH000667. <https://doi.org/10.1029/2025JH000667>

Received 4 MAR 2025

Accepted 3 AUG 2025




## Author Contributions:

**Conceptualization:** N. E. Glatt-Holtz, R. A. Harris, J. Krometis, H. Ringer, J. P. Whitehead  
**Data curation:** Y. Kurniawan, J. P. Whitehead  
**Formal analysis:** N. E. Glatt-Holtz, A. J. Holbrook, J. Krometis, Y. Kurniawan, H. Ringer, J. P. Whitehead  
**Funding acquisition:** J. P. Whitehead  
**Investigation:** J. Krometis, H. Ringer, J. P. Whitehead  
**Methodology:** J. Krometis, H. Ringer, J. P. Whitehead  
**Project administration:** R. A. Harris, J. Krometis, J. P. Whitehead  
**Resources:** J. P. Whitehead  
**Software:** J. Krometis, H. Ringer, J. P. Whitehead  
**Supervision:** J. Krometis, J. P. Whitehead

© 2025 The Author(s). *Journal of Geophysical Research: Machine Learning and Computation* published by Wiley Periodicals LLC on behalf of American Geophysical Union.

This is an open access article under the terms of the [Creative Commons Attribution License](https://creativecommons.org/licenses/by/4.0/), which permits use, distribution and reproduction in any medium, provided the original work is properly cited.

# Embracing Uncertainty in “Small Data” Problems: Estimating Earthquakes From Historical Anecdotes

N. E. Glatt-Holtz<sup>1,2</sup>, R. A. Harris<sup>3</sup>, A. J. Holbrook<sup>4</sup>, J. Krometis<sup>5,6</sup> , Y. Kurniawan<sup>7</sup>, H. Ringer<sup>6</sup> , and J. P. Whitehead<sup>8</sup> 

<sup>1</sup>Department of Statistics, Indiana University, Bloomington, IN, USA, <sup>2</sup>Department of Mathematics, Indiana University, Bloomington, IN, USA, <sup>3</sup>Department of Geological Sciences, Brigham Young University, Provo, UT, USA, <sup>4</sup>Department of Biostatistics, University of California Los Angeles, Los Angeles, CA, USA, <sup>5</sup>National Security Institute, Virginia Tech, Blacksburg, VA, USA, <sup>6</sup>Department of Mathematics, Virginia Tech, Blacksburg, VA, USA, <sup>7</sup>Department of Physics, Brigham Young University, Provo, UT, USA, <sup>8</sup>Department of Mathematics, Brigham Young University, Provo, UT, USA

**Abstract** Seismic risk estimates are greatly improved with an increased understanding of historical (and pre-historical) seismic events. Although Bayesian inference has been shown to provide reasonable estimates of the location and magnitude of historical earthquakes from anecdotal tsunamigenic evidence, the validity and robustness of such an approach has yet to be definitively demonstrated. Thus, in this article we present a careful analysis of the uncertainty inherent to this statistical recreation of historical seismic events. Using a priori estimates on the posterior and numerical approximations of the Hessian, we demonstrate that the 1852 Banda Sea earthquake and tsunami is well-understood given certain explicit hypotheses. Using the same techniques we also find that the 1820 south Sulawesi event may best be explained by a dual fault rupture, best attributed to the Kalatua fault potentially conjoining the Flores thrust and Walanae/Selayar fault.

**Plain Language Summary** Modern Bayesian statistical methods are shown to yield reasonable estimates on the location and magnitude of historical earthquakes using only anecdotal accounts of the subsequent tsunamis. This uncertain or “small” data can be used only if the uncertainty underlying it is well understood. We present some novel approaches that quantify this uncertainty, and demonstrate that even data of this anecdotal nature can be useful for the assessment of potential future earthquake hazards.

## 1. Introduction

The geologically recent mega-thrust earthquakes and giant tsunamis in Indonesia (2004) and Japan (2011) as well as the seismic catastrophes in Haiti (2010) and China (2008) all occurred in regions previously mapped as having “low” seismic hazard. One reason for this is because hazard assessments relied largely on instrumental data only available since the mid-1900s (Stein et al., 2012). Historical records and geological evidence of seismic events exist in each of these regions, but they were not adequately accounted for due to the uncertainty that is inherent to such data sources (Musson & Jiménez, 2008). For example, tsunami deposits were documented on the Sendai Plain before the 2011 Japan mega-thrust earthquake (Minoura et al., 2001), but were not considered in risk assessments, such as the retrofitting of the nuclear power plant. These recent seismic and tsunami disasters motivate us to push beyond the geologically limited time window of instrumentally recorded earthquakes to find new ways of quantifying unconventional data sources for earthquake locations and magnitudes.

Recent advances in sensing technology and rapid progress in data management and modeling has made it so that “big data” is an essential part of modern seismology (Arrowsmith et al., 2022) as well as many other sub-fields of geophysics (Yu & Ma, 2021) that is in concert with a significant portion of modern scientific inquiry. Yet there is no escaping the fact that the temporal scale of seismic activity far exceeds the resolution of modern instruments. “Big data” methods such as machine learning technologies that perform remarkably well at classification and reduced-cost approximate simulation tasks (Kong et al., 2019; Mousavi & Beroza, 2023), are incapable of breaching the gap in temporal scale for seismology precisely because the data of interest are sparse, irregular, and far too uncertain for these “big data” techniques. This illustrates a situation we will refer to as a “small data problem” wherein the observable data are so anecdotal, uncertain or noisy, that modern “big data” techniques such as neural networks, are infeasible.

**Validation:** N. E. Glatt-Holtz, A. J. Holbrook, J. Krometis, Y. Kurniawan, H. Ringer, J. P. Whitehead  
**Visualization:** J. Krometis, Y. Kurniawan, H. Ringer  
**Writing – original draft:** R. A. Harris, J. Krometis, J. P. Whitehead  
**Writing – review & editing:** N. E. Glatt-Holtz, A. J. Holbrook, J. Krometis, Y. Kurniawan, J. P. Whitehead

Resilience to tsunamis and other seismic hazards requires learning from what has happened in the geological past (UNISDR, 2009). Evidence of previous earthquake and tsunami events can be found in the geological record, such as deposits left by previous tsunami events (Sulaeman et al., 2017), damage to coral reefs (Gagan et al., 2015; Meltzner et al., 2010), and sediment cores of turbidites (Goldfinger et al., 2003). Additional information on past events is also available in the form of textual accounts in historical records such as the Wichmann catalog (Harris & Major, 2016; Wichmann, 1918, 1922) and other sources (Bergsma, 1868; Musson, 2012; Reid, 2012; Reinwardt, 1858) for Indonesia (see S. S. Martin et al. (2022) for a comprehensive catalog for the Indonesian archipelago), North and South America (see Singh et al. (1981); del Villar (2004); Kovach and Kovach (2004) e.g.), and many other locations in Asia and throughout the world. For these data we have seen a shift from the question “can we quantify what happened?” to “can we make a principled estimate of the uncertainties around what happened?”

Previous efforts to reconstruct pre-instrumental earthquakes have varied from a focus on the use of geological evidence (see, for example, Monecke et al. (2008); Sieh et al. (2008); Jankaew et al. (2008); Meltzner et al. (2010)) to the use of historically recorded (but not instrumental) accounts (Okal & Reymond, 2003; Bryant et al., 2007; Liu & Harris, 2014; Harris & Major, 2016; Reid, 2016; T. L. Fisher & Harris, 2016; Griffin et al., 2018; Cummins et al., 2020; Pranantyo & Cummins, 2020) as well as some combination of the two types of uncertain data (see S. S. Martin et al. (2019) for one example). Most of these efforts, particularly those directed toward using historical records, have relied on a combination of physical intuition and a restricted number of forward simulations of sophisticated numerical models for the seismic slip and corresponding tsunami to match the observational data. Qualitative comparisons are then made to the historical (or geological) record, and a heuristic choice is made as to the “best” forward simulation that fits the data.

In this paper, we analyze the problem of reconstructing historical earthquakes from accounts of tsunamigenic impact using a Bayesian framework (Gelman et al., 2014; Kaipio & Somersalo, 2005; Stuart, 2010; Tarantola, 2005). The Bayesian perspective is a natural fit because the chief problem we face is uncertainty in the data; the resulting posterior distribution will therefore provide estimates of the most likely values of but also the uncertainties that surround, the seismic parameters we would like to estimate, for example, the magnitude and location of the historical earthquake in question. Here the numerical resolution of partial differential equations (PDEs) describing tsunami wave propagation provides a “forward map” that can be “inverted” to adequately estimate the posterior distribution. Although the Bayesian framework has been used in the past to address problems in seismicity (see Bui-Thanh et al. (2013); J. Martin et al. (2012); Giraldi et al. (2017) for a few examples), the approach first outlined in Ringer et al. (2021) and further used in Paskett et al. (2024), Wonnacott et al. (2024) is the first that we know of to apply this methodology to pre-instrumental seismic events. Using numerical approximations of the Hessian of the computed posterior distribution and a priori bounds on perturbations of that distribution, we demonstrate that the previously published results are in fact statistically robust, and under the hypotheses proposed, provide a reasonable estimate of the posterior distribution of the causal earthquake. This provides key information on the utility of the previously obtained results and quantifies most of the uncertainty in the historical seismic inverse problem.

## 2. The Data: Historical Accounts of Tsunamis

Although there is a significant amount of geological evidence of tsunamis and earthquakes (see, e.g., Goldfinger et al., 2003; Gagan et al., 2015; Meltzner et al., 2010; Martin et al., 2022; Sulaeman et al., 2017), we will focus here on historical records of tsunami impact alone, as the uncertainties in such observations, while significant relative to modern seismometers, are significantly less than geological data or historical accounts of earth shaking. Very recently, the catalog Gempa Nusantara (Martin et al., 2022) was published, which includes references to historical accounts of tsunami and earthquake events throughout the Indonesian archipelago. This catalog coupled with Arthur Wichmann's *The Earthquakes of the Indian Archipelago* (Harris & Major, 2016; Wichmann, 1918, 1922) provides as accurate a documentation as can be expected for these historical events. The two events focused on in this report are drawn primarily from the Wichmann catalog (see Paskett et al., 2024; Ringer et al., 2021 for more details on each particular event). As an explicit example, consider the textual account below, which describes the impact of a tsunami at Banda Neira island located in the center of the Banda Sea.

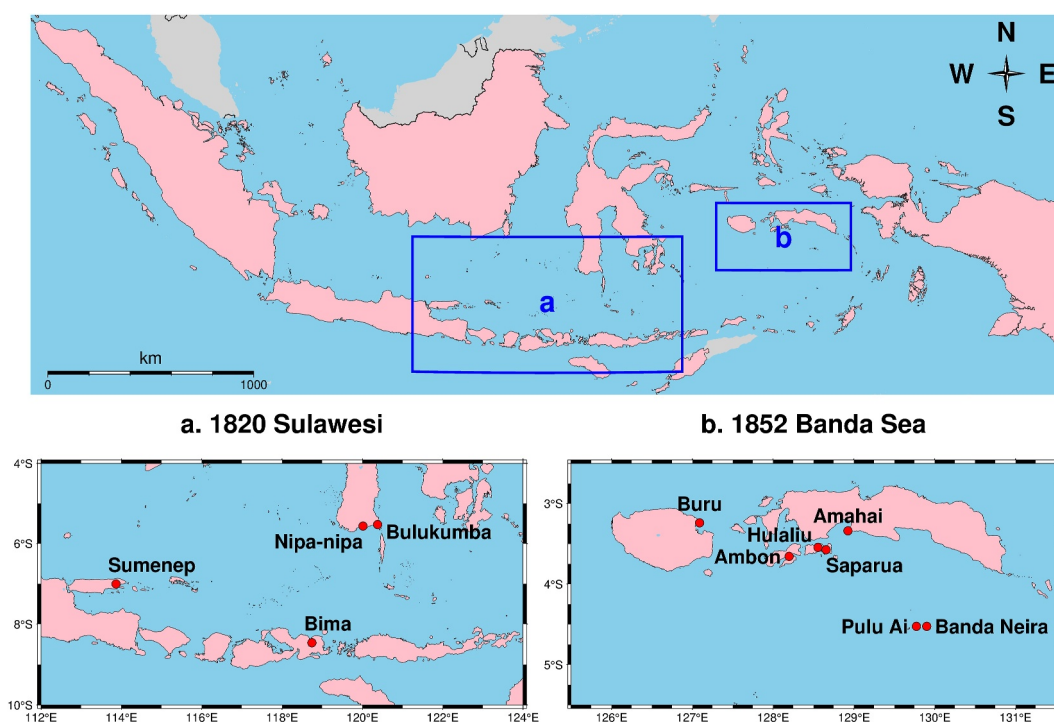


**Figure 1.** The two geographical regions of study referred to in this article. The labeled locations are the observation locations where the historical record provides anecdotal accounts of tsunami impact.

### 1852, November 26, 7:40

At Banda Neira, barely had the ground been calm for a quarter of an hour when the flood wave crashed in ...The water rose to the roofs of the storehouses ...and reached the base of the hill on which Fort Belgica is built on.

This excerpt from the Wichmann catalog provides clear descriptors, such as the location, arrival time, wave height, and inundation length that can be used to characterize the tsunami and infer the earthquake that might have caused it. Moreover, because historical observations of the tsunamis were observed in multiple, often geographically dispersed locations (Banda Neira being just one of several for the 1852 event), even uncertain observations can be “triangulated” to provide more certain estimates of earthquake size and location.

At the same time, the excerpt also demonstrates some of the challenges associated with doing such an inference in a rigorous way: Given that these measurements were taken well before the modern era of automated and sophisticated sensing, how accurate are they? What does water rising to rooftops tell us about the event? We approach these questions for two specific events in Indonesia whose geographic extent is depicted in Figure 1.

## 3. Methods

### 3.1. Bayesian Inference

The approach taken in Ringer et al. (2021) and Paskett et al. (2024) to leveraging the data described in Section 2 in a more principled and systematic fashion uses a Bayesian framework (Dashti & Stuart, 2017; Gelman et al., 2014; Kaipio & Somersalo, 2005; Tarantola, 2005), which provides a rigorous, statistical methodology for converting uncertain outputs into probabilistic estimates of model parameters. Although the Bayesian approach is not novel, and is in fact in use throughout the Geosciences more generally, we elaborate on its application in this setting in

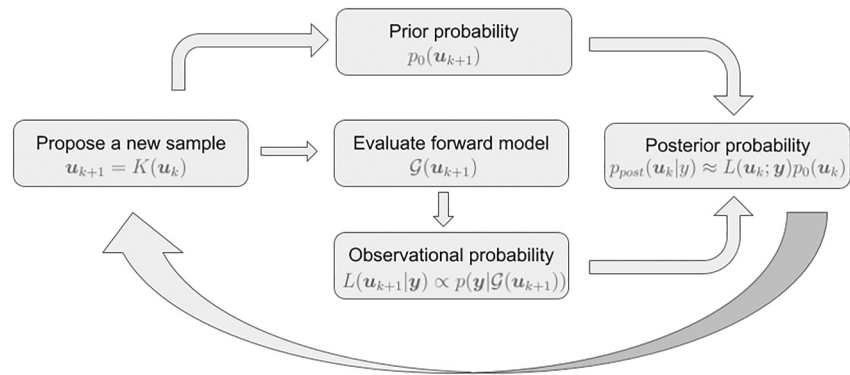


**Figure 2.** A block diagram of the MCMC process with the role of the prior and likelihood presented. Note that  $K(u_k)$  refers to the proposal kernel that moves the chain from one sample to the next based on the calculated prior and likelihoods for the previous sample.

great detail to highlight the novelty in Ringer et al. (2021) of applying the Bayesian formulation (coupled with data augmentation for the likelihood) to provide statistical estimates of past seismic events with only anecdotal observations. The power in using the Bayesian approach to the inverse problem arises from two key points: (a) Bayes' theorem allows us to use prior knowledge about the possible faults in the region in addition to the observations from the historical record. (b) Using inverse sampling methods we can construct an approximation to an entire probability distribution, which represents the solution to the inverse problem, and this posterior probability distribution will incorporate as much uncertainty as we desire to place in the observations and/or forward model. In other words, we are not restricted to providing a single pointwise estimate of the most probable earthquake to match the data, but we draw from a probability distribution that best matches that data and expert knowledge about the possible sources.

The primary contribution of the present article is a statistical analysis of the resulting posterior; however, in the following we also present a general formulation of the Bayesian inverse problem that generalizes the approach taken in Ringer et al. (2021), Paskett et al. (2024). To summarize the sampling procedure, refer to Figure 2, which depicts the an individual step through MCMC. The code used both for the Bayesian inversion, and the subsequent statistical analysis, which is the focus of this article is available at Whitehead (2025).

We note that although we use the pre-instrumental earthquake-tsunami problem as a motivating example, the framework described in this section is applicable to any problem where the “data” is “small”, that is, sparse and/or highly uncertain. In other words we are focused precisely on those settings where the observations alone are infrequent (either spatially or temporally) and potentially anecdotal. In what follows, we denote the model parameters characterizing the seismic event of interest by  $\mathbf{u}$ , the “data” by  $\mathbf{y}$ , the prior measure by  $p_0$ , the forward model  $\mathcal{G}$  from model parameters (e.g., earthquake magnitude and location) to observables (e.g., tsunami wave height), the likelihood by  $L(\mathbf{u}; \mathbf{y}) \propto p(\mathbf{y}|\mathbf{u})$ , and the posterior measure by  $p_{post}$ . See the references above for definitions of these quantities.

Bayes' theorem provides an explicit expression for  $p_{post}$  as

$$p_{post}(\mathbf{u}|\mathbf{y}) \propto L(\mathbf{u}; \mathbf{y})p_0(\mathbf{u}). \quad (1)$$

Most critically, the Bayesian approach incorporates uncertainty at all levels of the inverse problem, an essential feature given that the data in this case clearly does not provide enough information to fully specify the model parameters—we hope that it will tell us something about the parameters, but expect that it will necessarily not tell us everything.

### 3.2. Likelihood Modeling

In this section, we outline our procedure for modeling noisy or anecdotal data via the likelihood. Although the tsunami observations described in Section 2 provide a motivating example, and as pointed out above, the approach described here is applicable to any setting where the data are ill-defined or anecdotal but there is a

reasonable (in terms of computational expense and physical accuracy) forward model of the problem. Specific application to pre-instrumental seismic events in Indonesia are detailed in Ringer et al. (2021), Paskett et al. (2024), Wonnacott et al. (2024) but the presentation here is more general than any of those sources. The description below is different than those earlier works but presents a general framework that subsumes those descriptions.

To model the observational data  $\mathbf{y}$  from anecdotal observations such as those described in Section 2, we adopt a data augmentation approach that to date has not been utilized in this type of seismic setting to our knowledge (see, e.g., Albert & Chib, 1993; Holbrook et al., 2022; Tanner & Wong, 1987; Van Dyk & Meng, 2001) and introduce an auxiliary variable  $\mathbf{w}$  representing additional unobserved data. Then the likelihood is given by

$$L(\mathbf{u}; \mathbf{y}) \propto p(\mathbf{y}|\mathbf{u}) = \int p(\mathbf{y}|\mathbf{w}, \mathbf{u})p(\mathbf{w}|\mathbf{u}) d\mathbf{w}. \quad (2)$$

Here, for our augmentation variable  $\mathbf{w}$  we use the true value of the output (e.g.,  $w_i$  might be the true wave height, whereas  $y_i$  is the observed or recorded value of the wave height) and assume that uncertainty in the true value is independent of the unknown earthquake parameters  $\mathbf{u}$  so that  $p(\mathbf{y}|\mathbf{w}, \mathbf{u}) = p(\mathbf{y}|\mathbf{w})$ .

This leads to the evaluation of the posterior as:

$$p_{\text{post}}(\mathbf{u}|\mathbf{y}) = \frac{(\int p(\mathbf{y}|\mathbf{w})p(\mathbf{w}|\mathbf{u}) d\mathbf{w}) p_0(\mathbf{u})}{\int (\int p(\mathbf{y}|\mathbf{w})p(\mathbf{w}|\mathbf{u}) d\mathbf{w}) p_0(\mathbf{u}) d\mathbf{u}}.$$

From a philosophical standpoint, this strategy represents an application of the likelihood principle (Fisher, 1922; Casella & Berger, 2021).

Meanwhile, we require that true observations  $\mathbf{w}$  match the forward map  $\mathcal{G}(\mathbf{u})$  (in the historical tsunami setting the forward map is implemented via the Geoclaw software package (LeVeque et al., 2011)), so we define

$$p(\mathbf{w}|\mathbf{u}) = \delta(\mathbf{w} - \mathcal{G}(\mathbf{u})), \quad (3)$$

where  $\delta$  is the Dirac distribution centered at zero. Then plugging (Equation 3) into (Equation 2) yields

$$L(\mathbf{u}; \mathbf{y}) \propto \int p(\mathbf{y}|\mathbf{w})\delta(\mathbf{w} - \mathcal{G}(\mathbf{u})) d\mathbf{w} = p(\mathbf{y}|\mathcal{G}(\mathbf{u})). \quad (4)$$

The construction of the likelihood in Ringer et al. (2021) and Paskett et al. (2024) directly constructed a probability distribution for  $p(\mathbf{y}|\mathcal{G}(\mathbf{u}))$ . In the sequence we will most often follow the same convention, subsuming the auxiliary variable  $\mathbf{w}$ . The construction described here describes a general framework that both includes the presentation from those previous works, and outlines how data augmentation can be used for other “small data” problems.

To compare this with a more standard representation (in a setting distinct from the seismic inversion studied in this article), assume the data model  $\mathbf{y} = \mathbf{w} + \eta$  for additive observational noise where  $\eta \perp \mathbf{u}$  and  $\mathbf{w} = \mathcal{G}(\mathbf{u})$  for some  $\mathbf{u}$ . Denoting the probability density of  $\eta$  by  $p_\eta$ , we see that  $\mathbf{w}$  has density  $p(\mathbf{y}|\mathbf{w}) := p_\eta(\mathbf{y} - \mathbf{w})$  and via (Equation 4),

$$L(\mathbf{u}; \mathbf{y}) = p_\eta(\mathbf{y} - \mathcal{G}(\mathbf{u})). \quad (5)$$

This is precisely a popular likelihood used in Bayesian inverse problems; (see, e.g., Kaipio & Somersalo, 2005, Section 3.2.1 or Dashti & Stuart, 2017, Section 1.1). Hence, the auxiliary variable formulation above is a generalization of the standard likelihood model where the structure of the observational noise is left in a more implicit form, that is, it is not necessarily additive nor orthogonal to the input of the model, which is exactly the case for the anecdotal data considered in the present article. We do note that even though the observational noise is only implicitly defined via data augmentation, we still specify an explicit form for the likelihood (up to the level of



the forward model) by selecting probability distributions that are meant to capture (Equation 5). Deviating from a likelihood specified by restrictions on the noise distribution allows us to represent both the uncertainty due to the anecdotal nature of the observations, and the uncertainty from model assumptions, all within the likelihood framework.

Of course, the choice of the observation distribution  $p(\mathbf{y}|\mathbf{w})$  (and hence the likelihood  $p(\mathbf{y}|\mathcal{G}(\mathbf{u}))$ ) is subjective, as any interpretation of the historical records described in Section 2 must be. However, the approach outlined above represents a clear improvement over the modeling of the historical data as a single numerical value in at least two ways:

- By using probability distributions rather than single values, the methodology more clearly encapsulates the uncertainty associated with the observations.
- Modeling assumptions are explicitly specified and incorporated into the methodology so that the results are rigorous and reproducible.

One might interpret the direct modeling of the likelihood distribution as repeating a deterministic approach to the inverse problem a large number of times, with the observation distribution  $p(\mathbf{y}|\mathbf{w})$  representing the probability that a given modeler might interpret the observation as representing the true value  $\mathbf{w}$ . As pointed out above, this interpretation allows us to place estimates on the uncertainty due to the anecdotal nature of the observations.

In any case this represents a fruitful paradigm shift from the usual Bayesian inversion framework of selecting orthogonal, Gaussian noise by allowing more direct application to problems where observational signals and noise are inextricably intertwined. A practitioner can simply model what the observations tell them via  $p(\mathbf{y}|\mathbf{w})$  and then proceed with the usual Bayesian inference using the likelihood in (Equation 4). A direct extension of the current work would be to implement this approach for other types of geological evidence such as coral uplift, sediment cores, and disrupted turbidites, but the overall framework can be leveraged by problems outside of seismic inversion as well. From a more methodological perspective, a thorough comparison of this modern Bayesian approach with the Data Consistent Inversion method (Butler et al., 2014, 2018, 2020; Butler & Hakula, 2020; del Castillo-Negrete et al., 2024) that has been shown to adequately handle both aleatoric and epistemic uncertainty, would be very fruitful.

The full likelihood for the tsunami-earthquake inversion problem is complete with the specification of the forward model. The forward model in this case maps the earthquake parameters that model the resulting seafloor deformation via the Okada model (Okada, 1985), and then simulates the generation and propagation of the resultant tsunami to produce wave arrival times, wave heights, and inundation lengths at the observation locations. This is accomplished using the GeoClaw software package (Berger et al., 2011; González et al., 2011; LeVeque et al., 2011; LeVeque & George, 2008).

### 3.3. A Prior Distribution, and Posterior Sampling via Markov Chain Monte Carlo

The prior distribution for the historical seismic investigation considered here is a probability distribution that describes the probable earthquake parameters that are physically feasible for the event in question. Specific details are contained in Ringer et al. (2021) and Paskett et al. (2024), but we summarize the construction of the prior here. The prior distribution on magnitude for both events was taken from the Gutenberg-Richter distribution (see Gutenberg & Richter, 1955, 1956), truncated to reasonable maximum (9.5) and minimum (6.5) values. The prior on the length, width, and slip of the earthquake were taken as fluctuations around a mean fitted value determined by magnitude, and dictated by historical earthquake data cataloged in Wells and Coppersmith (1994) and from recent major events from the global USGS data set (Bakun, 2002 (accessed 19 July 2020)). Offset values for the length and width were also established and a zero mean Gaussian prior was set for these values with variance specified by the mean squared error of the regressed fit.

For the 1852 Banda Sea earthquake, the latitude-longitude location, depth, and rough geometry of the underlying fault were specified using data from the Slab2 data set (Hayes et al., 2018) that incorporates modern instrumental data to map out major subduction zones globally. The prior distribution for the Banda Sea was selected to identify earthquakes with potential to generate significant tsunamis, that is, very deep events do not yield sufficient surface deformation for a landslide, but shallow earthquakes also do not have the ductile resistance to generate sufficient slip. Hence, the prior is set by prescribing a probability distribution on the depth of the earthquake centered at 30 km deep with a standard deviation of 5 km and truncated between 5 km and 50 km depth. This is mapped back

through the SLAB2.0 data set to identify the possible longitude-latitude coordinates for the earthquake centroid. A prior distribution on the depth off-set (fluctuations about the prescribed SLAB2.0 values) is specified as dictated by the uncertainty estimates in SLAB2.0 itself. Although the geometry of the Banda Arc is (at least for the seismic setting) well established, the primary concern with the prior for this event is that it restricts the possible source to a mega-thrust event on the Arc itself, that is, Ringer et al. (2021) does not consider the possibility of a submarine landslide or any other atypical source for the tsunami.

No such data set was available for either the Flores thrust or Walanae/Selayar. For the Flores thrust the prior geometry is modeled using a Gaussian process trained off of geologically recent events on the fault from the USGS catalog. There is a dearth of recent events for the Walanae/Selayar fault, so this is instead modeled as a planar slab with variations along the strike and dip angles (in addition to depth) provided for as additional sample parameters. The primary drawback in using the Gaussian process to model the Flores thrust is that this did not allow for any strict boundaries (such as keeping the earthquake on the correct side of the actual fault), and the available data were sufficiently sparse that the Gaussian processes were quite permissive. On the other hand, the prior distribution on the Walanae/Selayar fault is highly reliant on the expert opinion of the geologists involved on the project, that is, there were very little data to back up the hypothesized geometry beyond some general information on the formation of similar faults globally, and some much smaller seismic events to the north along the southern branch of Sulawesi island.

Resolving statistics—moments, correlations, marginals, and other credibly interesting sets, is a computationally arduous task. Effectively we are attempting to resolve integrals in 6–10 dimensions where each function evaluation requires the solution of a PDE defining the forward model (which parallelized across 24 cores takes between 2 and 20 min depending on the simulation parameters), and hence the likelihood. As such the only feasible approach is to use Markov Chain Monte Carlo (see Casella & Berger, 2021 e.g.). Here we use a classical random walk MCMC method since more advanced gradient based approaches (e.g., Hamiltonian Monte Carlo) would require infeasible gradient evaluations of  $G(u)$ . This does require the calculation of several tens of thousands of samples in order to adequately resolve the desired statistics.

We point out that the stochastic process we generate here via random walk MCMC can be considered a random walk through the seismic parameter space of possible events guided or constrained by the posterior distribution. This approach is thus well-suited to other situations where a reasonably accurate forward model exists and computational expediency is not essential (active seismic events are not viable problems for this framework as the time to results is critical). This random process through the parameter space is convenient a posteriori as it yields data that can be analyzed to give estimates on various statistics and observables that may be of interest to the user.

Chains, particularly when initialized in different regions of the parameter space, sometimes got stuck in places with low posterior probability. We therefore conducted periodic importance-style resampling according to posterior probability (see Doucet et al., 2001); this resampling does not maintain invariance with respect to the posterior measure, but provides a mechanism to “jump” trapped samples from poorly performing regions of the parameter space to regions given more weight by the posterior distribution. To minimize any bias from the resampling steps, the approximate posterior was ultimately assembled from samples collected after a suitable burn in period following the last resampling step.

### 3.4. Resolution and Properties of the MAP Point

There are traditional approaches to ensuring the convergence of MCMC such as trace plots, the Gelman-Rubin diagnostic (Gelman et al., 1992) and autocorrelation calculations, some of which have already been reported for the posterior distributions discussed here in Ringer et al. (2021), Paskett et al. (2024). All of these measures of the posterior provide global assurances that a sufficient number of samples have been collected. However, these measures do not provide information about the geometry of the posterior, which provides insight into the nature of the problem itself as illustrated below. Instead, here we present an alternative approach that identifies how well the posterior is approximated locally, which also yields insight into the nature of the inverse problem under consideration.

To verify that the posterior is adequately resolved, we focus on its geometry near the maximum a posteriori (MAP) value. If the distribution is adequately resolved then the MAP point will be a true maximum of the posterior distribution. Hence the gradient of the posterior will be zero, and as long as the distribution is

sufficiently smooth then the Hessian (matrix of second order derivatives) will be negative definite. As gradients are not available for the forward model  $\mathcal{G}$  then we resort to surrogates or approximations of the derivative of the full posterior. This is performed via the following approach outlined here (McClarren, 2018).

Let  $f$  be a function whose input is  $\theta = (\theta_1 \ \theta_2 \ \dots \ \theta_N)^T$  (in our context we will actually take  $\theta = \mathbf{u}$  to identify how the MAP point changes with perturbations in the unknown parameters themselves). Suppose there are  $M$  samples of  $\theta$ , that is we have  $M$  different possible inputs to  $f$ . Denote  $f^m = f(\theta^m)$  as the model output evaluated using the parameter sample  $\theta^m = (\theta_1^m \ \theta_2^m \ \dots \ \theta_N^m)^T$ . The Taylor series expansion of  $f^m$  around the specific set of inputs/parameters  $\tilde{\theta}$  is given by

$$f^m \approx f(\tilde{\theta}) + \sum_{n=1}^N \frac{\partial f(\tilde{\theta})}{\partial \theta_n} (\theta_n^m - \tilde{\theta}_n). \quad (6)$$

If we have  $M$  samples of  $\theta$  and correspondingly of  $f$ , then Equation 6 defines a set of  $M$  equations. These equations can be written compactly in matrix notation as

$$\mathbf{F} \approx \Phi \mathbf{d}, \quad (7)$$

where the entries of the vectors  $\mathbf{F}$ ,  $\mathbf{d}$  and matrix  $\Phi$  are given by

$$\begin{aligned} F_m &= f^m - f(\tilde{\theta}), \\ d_n &= \frac{\partial f(\tilde{\theta})}{\partial \theta_n}, \text{ and} \\ \Phi_{mn} &= \theta_n^m - \tilde{\theta}_n. \end{aligned}$$

The gradient of the function  $f$  at  $\tilde{\theta}$  can be approximated by solving Equation 7 for the vector  $\mathbf{d}$ .

We can extend Equation 6 to second order to yield a similar approach to estimate the second order derivatives as well, requiring an even larger number of samples  $M$  in order to yield a reasonable estimate of the resultant Hessian matrix. In this case the unknown vector will now include elements from both the Jacobian (gradient if  $f(\theta)$  is scalar valued) and the Hessian matrices. Solving this new linear problem yields an estimation of both the Jacobian and the Hessian that can be used to verify whether the MAP point is adequately resolved.

For the posterior distributions considered here, the parameters have different physical units (length of the earthquake rupture is in thousands of kilometers whereas the slip length is in meters for example), and thus they have a significantly different range of values meaning that the estimated derivative will be unnecessarily skewed if computed in the original physical units. To avoid this potential pitfall when estimating the derivative, we scale the sample parameters  $\theta$  from the posterior distribution (as sampled via MCMC) by the standard deviation across the entire sampled posterior, which yields unitless parameter samples (Helton et al., 2006; Mortenson et al., 2023).

In order to obtain a good estimation of the derivative, we want to use samples  $\theta^m$  that are not too far from the estimation point of interest  $\tilde{\theta}$  in the estimation, that is, the MAP point, but tuning the “closeness” of this points is a difficult task. Hence, we use the first derivative condition to tune this calculation, and then use the second derivative condition as a diagnostic tool. To be specific we define a hyper-sphere of radius  $r$  in the scaled parameter space around the MAP point and only use the parameter samples that are located inside this hyper-sphere, which provides the hyperparameter  $r$  that is selected to give the most reasonable first derivative approximation. Large values of  $r$  includes samples that are far from the MAP point, which will skew the derivative approximation, whereas small values of  $r$  give too few samples in the regression, in either extreme the derivative estimation will be inaccurate. We choose an  $r$  value that minimizes the norm of the gradient of the posterior at the MAP point, that is, we are relying on the assumption that the MAP point truly is a local maximum of the posterior, that is, a critical point to identify the critical value of  $r$ .



Once the critical value of  $r$  is identified that best agrees with the first derivative condition at the MAP point, then we use that value to compute an approximated Hessian and evaluate if the approximated Hessian is indeed negative semi-definite. Not only does a fully negative semi-definite Hessian indicate that the MAP point is truly a maximal probability value, but the dominant eigenvectors of the Hessian also inform us which direction the probability will change most easily moving away from the MAP point (Mannakee et al., 2016). This means that we can determine which parameters of the system are most sensitive to perturbation away from the MAP point.

### 3.5. Error Bounds and Sensitivity of the Posterior Distribution

Given the necessarily uncertain process of interpreting textual records as probability distributions, it would be natural to question how sensitive the results are to different choices of the observation distribution. To allay some of these concerns, in this section we describe the computation of upper and lower bounds on the potential error in the posterior distribution due to the choice of likelihood, specifically the selected parameterization of the observational probability distributions. In other words, we produce numerically estimated bounds (based on rigorously justified assumptions) that indicate that small perturbations in our choice of the observational probability distributions and/or parameterizations of the prior, will not drastically affect the structure of the resultant posterior distribution, that is, the posterior itself is not overly sensitive to the assumptions made in the setup described here and hence we get a reasonable grasp on the uncertainty present in the problem. We also provide information as to which portions of the data or other choices in the modeling most affect the resulting posterior. In other words, sensitivity also provides an indication of which parts of the historical account most or least constrain the uncertainty.

To develop these bounds, we use three theoretical results from Dupuis et al. (2016), which provides various bounds on estimates derived from probability distributions as those distributions are perturbed. First, we use a second order estimate for the relative entropy (Kullback-Leibler divergence)  $\mathcal{R}$  between a distribution  $P^\theta$  and its perturbation  $P^{\theta+v}$  (see Dupuis et al., 2016, Equation 2.35):

$$\mathcal{R}(P^{\theta+v}||P^\theta) = \frac{1}{2}v^T \mathcal{I}(P^\theta) v + \mathcal{O}(|v|^3), \quad (8)$$

where  $\mathcal{I}$  is the Fisher information matrix (FIM). The  $\mathcal{I}$  that we specify here corresponds to a measurement of the dependence of information contained in the posterior, on the specific parameters  $\theta$  (such as mean and variance of a normal distribution, specifically note that these  $\theta$  here are *NOT* elements of  $\mathbf{u}$  the unknown earthquake parameters) selected to create the observational probability distributions, which then define the likelihood (when coupled with the forward model).

The second estimate on the perturbation of a probability measure utilizes the following bound on the expected value of an observable  $f$  (an observable in this context is any variable continuously drawn from the posterior, i.e., the resultant earthquake parameters are one example, so that  $f$  can be viewed as an element of  $\mathbf{u}$ ) with respect to the probability measure  $Q$  in terms of the values of  $f$  according to the probability measure  $P$  (Dupuis et al., 2016, Equation 2.11):

$$\begin{aligned} \sup_{c>0} \left( -\frac{1}{c} \log \mathbb{E}_P [e^{-c(f - \mathbb{E}_P[f])}] - \frac{1}{c} \mathcal{R}(Q||P) \right) \\ \leq \mathbb{E}_Q[f] - \mathbb{E}_P[f] \leq \inf_{c>0} \left( \frac{1}{c} \log \mathbb{E}_P [e^{c(f - \mathbb{E}_P[f])}] + \frac{1}{c} \mathcal{R}(Q||P) \right). \end{aligned} \quad (9)$$

Here  $\mathbb{E}_P$  and  $\mathbb{E}_Q$  are the expected values according to models  $P$  and  $Q$ , respectively, and  $Q$  is assumed to be absolutely continuous with respect to  $P$  (i.e.,  $P(A) = 0 \Rightarrow Q(A) = 0$  for any event  $A$ ). By letting  $P$  be the posterior measure, we can estimate the uncertainty in observables with respect to other probability measures  $Q$ , which are “close” to the estimated posterior  $P$ , that is, we can estimate how much slight changes in the posterior would affect the observables we care about.

The expressions inside the sup and inf in (Equation 9) can be differentiated to find the value of  $c$  that provides the optimal bound for a given value of  $\mathcal{R}(Q||P)$ . When  $f$  is bounded, the equations also give a global upper and lower bound  $\mathbb{E}_Q[f]$ . Details of these derivations are reserved for Appendix B. By combining these inequalities with

**Table 1**  
*Summary of MCMC Parameters Used to Estimate Posterior Distributions*

Event	Fault	Chains	Initial conditions	Total samples (after burn-in)
1852 Banda Arc	N/A	14	7	70,000
1820 Sulawesi	Flores	10	5	127,690
1820 Sulawesi	Walanae/Selayar	10	5	104,970

(Equation 8) (setting  $Q = P^{\theta+v}$ ), we provide approximate (in the sense that (Equation 8) is only valid in the limit as the perturbation is small) bounds on most likely earthquake parameters drawn from the posterior for perturbations of the observational distributions. To approximate the worst-case scenario (most sensitive to changes in the parameters), we assume a perturbation in the direction of the first singular vector of the FIM  $I$  i.e., directly computable from the MCMC data collected in Ringer et al. (2021) and Paskett et al. (2024). This dominant eigenvector is precisely the worst case perturbation in the linear regime, and should be a reasonable approximation for most small perturbations to the posterior measure.

Finally, (Dupuis et al., 2016, Equation 2.39) bounds the sensitivity of estimates of observables due to changes in the likelihood (more directly changes to the observational probability distributions, i.e., perturbations in  $\theta$ ):

$$|S_{f,v}(P^\theta)| \leq \sqrt{\mathbb{V}_{P^\theta}(f)} \sqrt{v^T I(P^\theta) v}. \quad (10)$$

Here  $f$  is an observable, which we will consider to be the selected earthquake parameters that are used to model the earthquake and hence tsunami (typically we use a variation of the Okada parameters Okada, 1985),  $\text{Var}$  denotes the variance, and the sensitivity bound  $S_{f,v}$  is the numerically approximated derivative of  $\mathbb{E}_{P^\theta}[f]$  with respect to a perturbation of  $\theta$  in the direction of  $v$ . Equation 10 shows that the greatest sensitivity will occur when the perturbation  $v$  heavily weights likelihood parameters  $\theta$  that most affect the posterior (the second term) and when earthquake parameters  $f$  (elements of  $\mathbf{u}$ ) have the most uncertainty in the posterior (the first term). To estimate the worst-case scenario, we again assume that the perturbation  $v$  is along the first singular vector of  $I$ . Such sensitivity bounds are computed for a 10% relative perturbation along this direction.

To define the perturbations to the observation and likelihood distributions that we consider, we must parameterize the observation distributions selected for each historical account. To do so, we fix the structure of the choice of  $p(\mathbf{y}|\mathbf{w})$ —for example, if the observational distribution is a normal distribution we continue to use a normal distribution—but let the parameters, denoted by  $\theta$ , be the parameters characterizing that distribution (for example, the mean and variance for a normal distribution).

## 4. Results

The approximation of the posterior distribution was performed via MCMC sampling for each event as described in Section 3.3. Because the 1820 Sulawesi tsunami was in the vicinity of two distinct faults, we conducted separate sampling for each. The specific details of the sampling and the resulting posterior parameter estimates are described in detail in Ringer et al. (2021) and Paskett et al. (2024) for the 1852 and 1820 events, respectively; a high-level summary of the MCMC parameters is provided in Table 1. There are three posterior distributions that we are concerned with in this article. Each posterior is constructed with either 14 or 10 individual MCMC chains. Each of these chains are initialized at roughly equally spaced geographic locations along the specific fault (5 each for the 1820 event and 7 each for the 1852 event). At each of these geographic locations, two chains are initialized at two different magnitudes:  $Mw8.5$  and  $Mw8.0$  (this high magnitude is selected to guarantee the chain is initialized with a finite log-likelihood). The last column in Table 1 details the total number of samples after an adequate burn-in time is allowed for each posterior distribution. Note that the 1852 Banda Arc event had many more samples collected, but there were only 70,000 samples after the last importance resampling step (see Section 3.3 for details).

This section is focused on additional analysis, beyond that in the above references, aimed at ascertaining whether the resulting posterior distributions are robust to the modeling assumptions—that is, whether the methodology in Section 3.2 has adequately addressed the uncertainty in the data described in Section 2. As described earlier, the

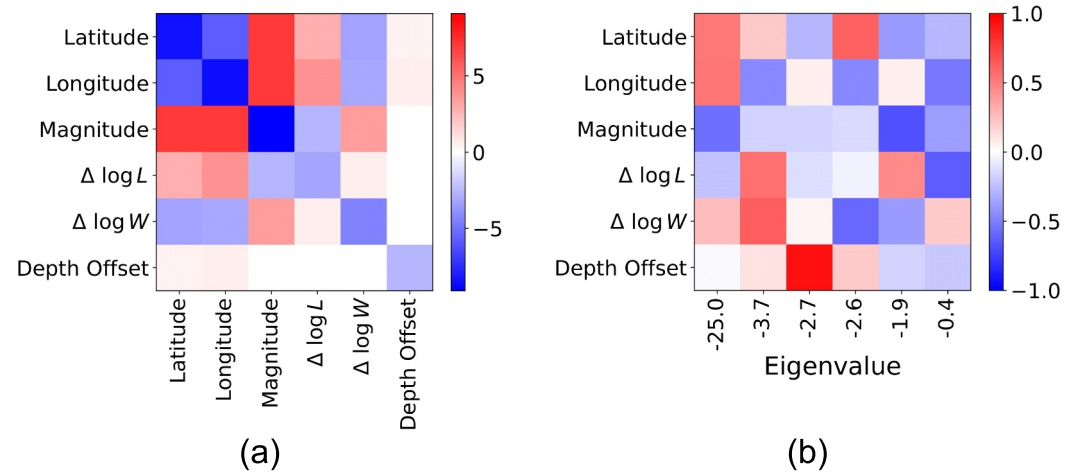


**Figure 3.** (a) Estimated Hessian of the non-normalized log-posterior and (b) the corresponding eigenvectors for the posterior distribution of the Banda 1852 event.

approach we take is to quantify the sensitivity of the final posterior distribution to the assumptions made in deriving the observational distributions. This certainly does not address all of the uncertainty in the existing data, but it does give significant information about the robustness of the modeling assumptions used to generate the posterior samples.

#### 4.1. Structure of the Posterior Distributions

To verify that the posterior distribution for each event was adequately resolved, we approximated the Hessian near the MAP point.

##### 4.1.1. 1852 Banda Sea

Figure 3 shows the Hessian of the non-normalized log-posterior approximated at the MAP point and the eigenvectors of the Hessian for the Banda 1852 posterior. The eigenvectors are presented as columns of the matrix of Figure 3b, with the corresponding eigenvalues listed on the horizontal axis. Although the Hessian matrix does not provide the absolute magnitude of the curvature near the MAP, it does demonstrate the relative curvature in different directions. Additionally, the eigenvalues indicate the relative sensitivity in each principle direction, for example, the dominant eigenvector is approximately  $25/3.7 \approx 6.75$  times more sensitive than the second most dominant eigenvector.

##### 4.1.2. 1820 Sulawesi

Figure 4 presents the same calculation as Figure 3, but now for the 1820 Sulawesi event. There are several noteworthy features of this calculation. Before discussing these issues, we note that the dimension of the posterior for the 1820 Sulawesi event is larger because we allowed for variations in the depth, that is, depth offset ( $\Delta d$ ), dip offset ( $\Delta \beta$ ), strike offset ( $\Delta \alpha$ ), and rake offset ( $\Delta \gamma$ ). Hence, the Hessian for the 1820 Sulawesi event is an  $9 \times 9$  matrix rather than the  $6 \times 6$  object identified in Figure 3 for the 1852 Banda Sea event.

#### 4.2. Error Bounds and Sensitivity of the Posterior

Tables 2 and 3 show our first set of sensitivity estimates derived using the methodology described in Section 3.5. First, for each  $\theta$  parameter we list the associated Fisher information (the diagonal element of the FIM). The FIM is here calculated with respect to the parameters that describe the observational probability distributions, that is, we are considering the sensitivity of the posterior with respect to the likelihood as specified through the observational probability distributions, as described in Section 3.2. The definition of the FIM and a derivation of it for the posterior for this problem are given in Appendix A. Because the differences in Fisher information for absolute changes in parameter values are largely driven by units (e.g., meters for wave height vs. minutes for arrival time),

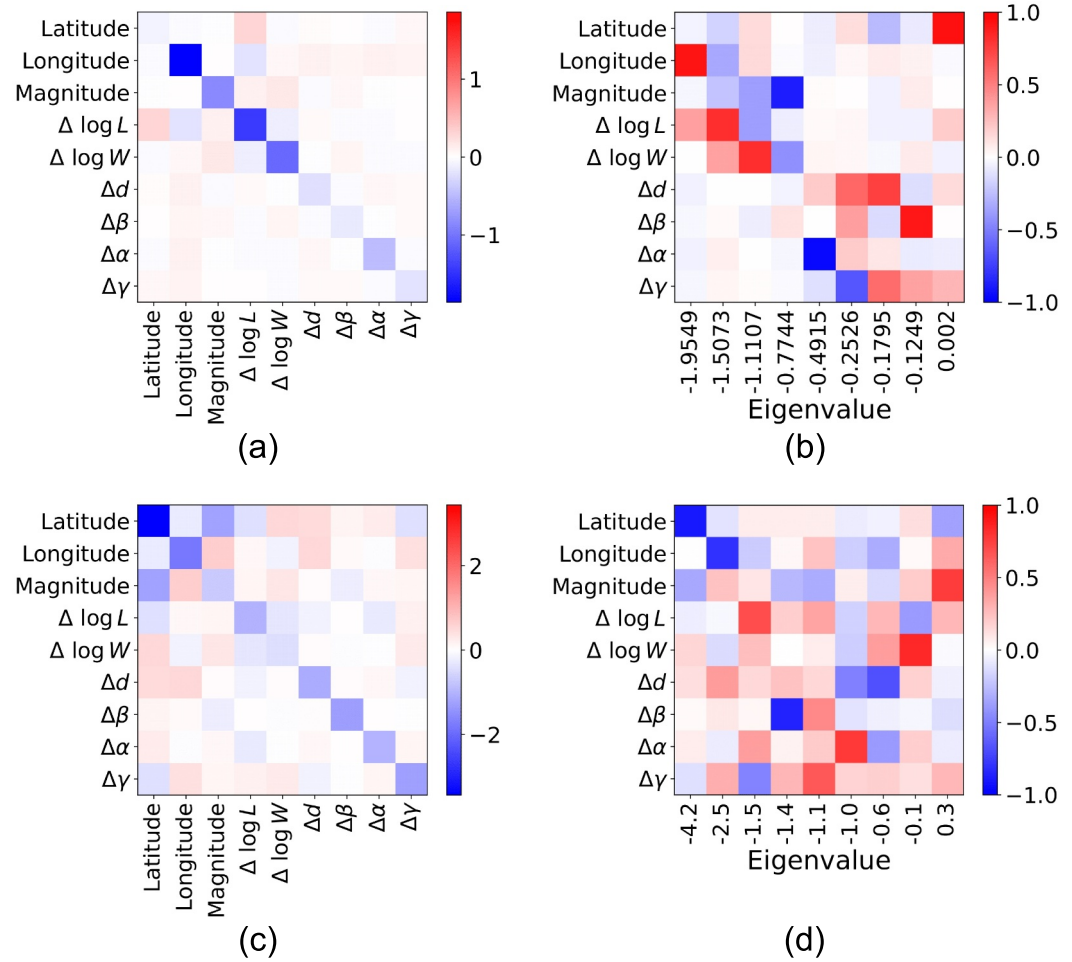


**Figure 4.** (a) Estimated Hessian of the non-normalized log-posterior and (b) the corresponding eigenvectors for the posterior distribution of the 1820 Sulawesi event, modeled with the Flores source. (c, d) Show the corresponding figures for the Walanae/Selayar source.

the Fisher information values presented in these tables are computed for the relative change in each parameter value.

Second, we present the relative entropy (Kullback-Leibler divergence)  $\mathcal{R}$  associated with a 10% shift in each parameter computed from (Equation 8). That is, for  $P^\theta$  we use the original posterior distribution as calculated in either Ringer et al. (2021) or Paskett et al. (2024); for the perturbation  $v$  for the  $i^{\text{th}}$  row in each table we set  $v_i = 0.1\theta_i$  and  $v_j = 0, j \neq i$ . As shown in Table 2, this measure indicates that the most sensitive parameter in the observational probabilities (and hence the likelihood) for the 1852 event is the specified mean for the arrival time at Saparua (value of 0.096), followed closely by the mean for the arrival time at Banda Neira (value of 0.07) and the specified mean for the wave height at Ambon (value of 0.068).

The relative entropy for a 10% perturbation for the 1820 event, shown in Table 3, does not provide as distinct of a selection of the most sensitive parameter for either seismic source. It does give some information on the approximated sensitivity of the posterior though. For the Flores source, the dominant sensitivity according to this metric arises from the specification of the standard deviation for the wave height observation at Bulukumba (value of 0.017) followed by the standard deviation of the arrival time at Bulukumba (value of 0.014), the specified mean of the arrival time at Sumenep (value of 0.012) and the specified mean of the wave height at Bulukumba (value of 0.01).

**Table 2**

*Observation Distribution Parameters for the 1852 Banda Sea Event, the Associated Fisher Information Values, Relative Entropy According to (Equation 8) Associated With a 10% Relative Perturbation, and the First (Most Sensitive) Singular Vector of the Fisher Information Matrix*

Location	Observation	Distribution	Parameter ( $\theta$ )	Value	FI	$\mathcal{R}$ 10%	Sing. Vec.
Pulu Ai	Height	Normal	Mean	3	5.934	0.030	−0.151
Pulu Ai	Height	Normal	Std	0.8	2.505	0.013	0.087
Ambon	Height	Normal	Mean	1.8	12.370	0.062	0.364
Ambon	Height	Normal	Std	0.4	5.220	0.026	0.216
Banda Neira	Arrival	Skewnorm	Mean	15	14.082	0.070	0.447
Banda Neira	Arrival	Skewnorm	Std	5	1.950	0.010	−0.148
Banda Neira	Arrival	Skewnorm	A	2	1.339	0.007	0.132
Banda Neira	Height	Normal	Mean	6.5	7.525	0.038	−0.014
Banda Neira	Height	Normal	Std	1.5	0.884	0.004	−0.006
Banda Neira	Inundation	Normal	Mean	185	2.663	0.013	−0.010
Banda Neira	Inundation	Normal	Std	65	0.272	0.001	−0.006
Buru	Height	Chi	Mu	0.5	0.006	0.000	0.009
Buru	Height	Chi	Sigma	1.5	0.122	0.001	0.035
Buru	Height	Chi	Dof	1.01	0.142	0.001	0.040
Hulaliu	Height	Chi	Mu	0.5	0.001	0.000	0.000
Hulaliu	Height	Chi	Sigma	2	0.003	0.000	−0.000
Hulaliu	Height	Chi	Dof	1.01	0.185	0.001	0.002
Saparua	Arrival	Normal	Mean	45	19.264	0.096	0.716
Saparua	Arrival	Normal	Std	5	1.280	0.006	−0.163
Saparua	Height	Normal	Mean	5	9.085	0.045	0.009
Saparua	Height	Normal	Std	1	0.869	0.004	−0.005
Saparua	Inundation	Normal	Mean	125	2.905	0.015	0.005
Saparua	Inundation	Normal	Std	40	0.178	0.001	−0.003
Kulur	Height	Normal	Mean	3	0.199	0.001	0.038
Kulur	Height	Normal	Std	1	0.362	0.002	−0.050
Ameth	Height	Normal	Mean	3	0.351	0.002	0.043
Ameth	Height	Normal	Std	1	0.409	0.002	−0.046
Amahai	Height	Normal	Mean	3.5	4.107	0.021	0.014
Amahai	Height	Normal	Std	1	0.784	0.004	−0.001

*Note.* The units of all height and inundation observations is in meters, and minutes for all arrivals.

The last column in Tables 2 and 3 lists the first singular vector of the FIM, which is the combination of perturbations of the observation parameters that produce the largest relative entropy—effectively a linearized “worst-case” perturbation, that is, this is yet another indicator of how changes in the observational probability parameters would most significantly affect the structure of the posterior. The key to interpreting these quantities is to recognize that this provides a direction along which the relative entropy will increase the most (at least for small perturbations); that is, the precise numbers provided here are less important than their values relative to each other.

To further investigate how changes to the likelihood will affect the posterior, we projected what effect a 25% shift in the parameters along the dominant singular vector will have on the mean value for the key earthquake parameters. Even for relatively large perturbations, we get relatively narrow bounds on posterior estimates. For example, even with a 25% perturbation in the most sensitive direction, the expected value of magnitude according to the perturbed posterior distribution would be between 8.7 and 9.0 for the 1852 Banda Sea event (see Figure 5), a



**Table 3**

Observation Distribution Parameters for the Sulawesi 1820 Event, Associated Fisher Information Values, Relative Entropy According to (Equation 8) Associated With a 10% Relative Perturbation, and the First (Most Sensitive) Singular Vector (Denoted SV) of the Fisher Information Matrix

Name	Observation	Parameter	Value	Flores			Walanae/Selayar		
				FI	$\mathcal{R}$ 10%	SV	FI	$\mathcal{R}$ 10%	SV
Bulukumba	Arrival	Mean	15	0.147	0.001	−0.062	3.039	0.015	−0.212
Bulukumba	Arrival	Std	10	2.723	0.014	−0.263	1.017	0.005	0.026
Bulukumba	Height	Mean	18	2.046	0.010	0.494	1.716	0.009	0.398
Bulukumba	Height	Std	5	3.305	0.017	−0.624	2.242	0.011	−0.446
Sumenep	Arrival	Mean	240	2.409	0.012	0.093	0.266	0.001	−0.049
Sumenep	Arrival	Std	45	1.108	0.006	−0.065	0.047	0.000	0.021
Sumenep	Height	Mean	1.5	0.481	0.002	0.132	0.125	0.001	0.084
Sumenep	Height	Std	1	0.072	0.000	−0.007	0.074	0.000	−0.063
Nipa-Nipa	Height	Mean	3	1.044	0.005	0.349	1.342	0.007	0.365
Nipa-Nipa	Height	Std	2	1.047	0.005	0.267	4.421	0.022	0.660
Bima	Height	Mean	10	1.253	0.006	0.191	0.326	0.002	0.066
Bima	Height	Std	4	1.088	0.005	−0.183	0.712	0.004	−0.097

Note. Note that all observation distributions were normal distributions.

very large earthquake in any case. The 1820 Sulawesi event doesn't yield quite as strict of bounds on the estimated values for either source, but the error bars in all requisite parameters still appear reasonable (see Figures 6 and 7). One caveat: As the size of the perturbation grows, the approximation in (Equation 8) will eventually break down.

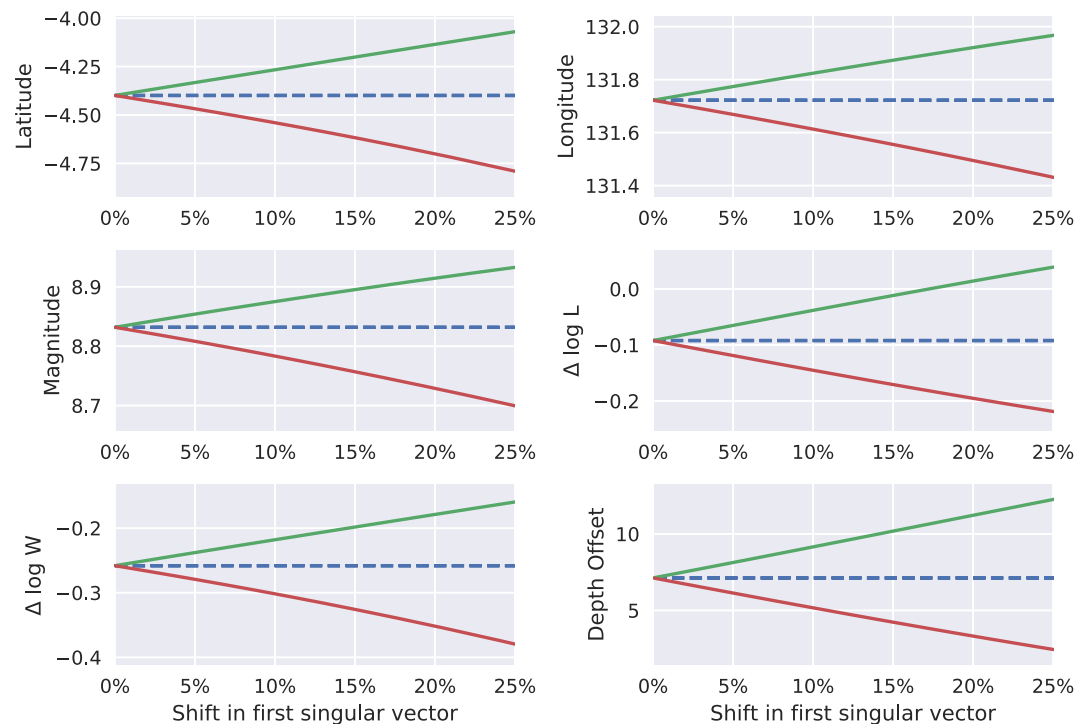


**Figure 5.** Bounds on mean parameter values in terms of relative perturbation in the first singular vector of the Fisher information matrix (see the last column of Table 2) for the 1852 Banda Sea earthquake event. Upper and lower bounds are in green and red, respectively. The posterior mean is in blue. The units for these plots are as follows: latitude and longitude (degrees), magnitude ( $M_w$ ), the  $\Delta$  parameters ( $\log(\text{km})$ ), and depth offset (km).

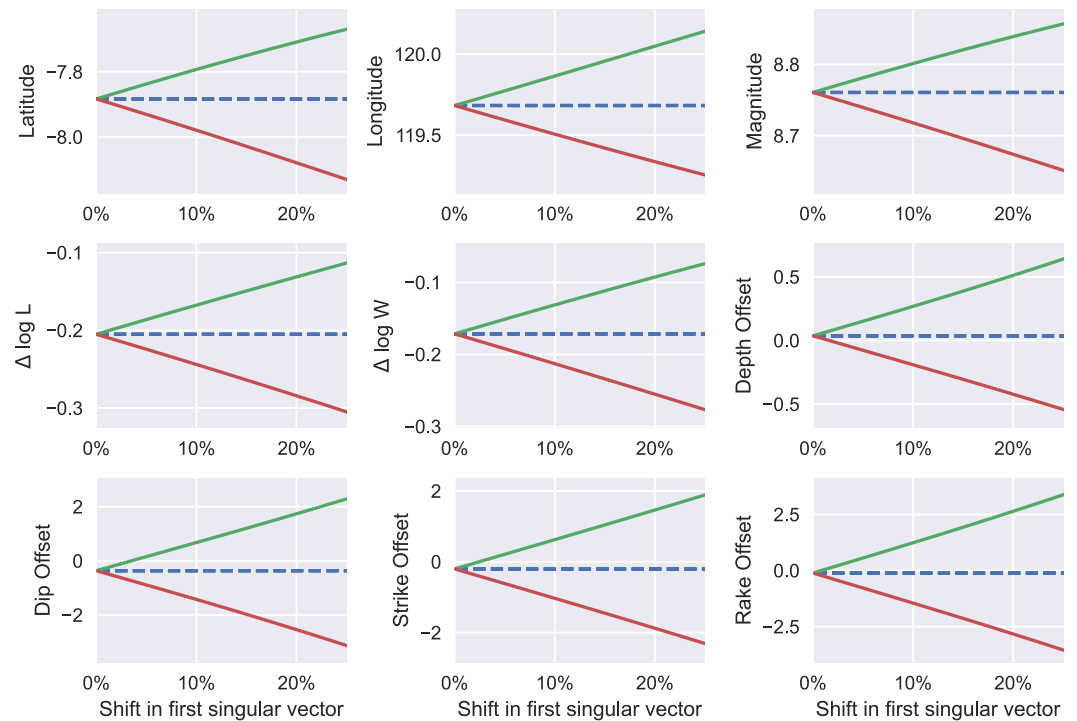


**Figure 6.** Bounds on mean parameter values in terms of relative perturbation in the first singular vector of the Fisher information matrix (see the SV columns of Table 3) for the 1820 Sulawesi event for the Flores source. Upper and lower bounds are in green and red, respectively. The posterior mean is in blue. The units for these plots are as follows: latitude and longitude (degrees), magnitude (Mw), the  $\Delta$  parameters (log(km)), depth offset (km), and the angular offsets in degrees ( $^{\circ}$ ).

In this case, we refer the reader to Figure B1, where the  $x$ -axis is in terms of relative entropy taken directly from (Equation 9).

A final set of estimates for the sensitivity of each posterior distribution with respect to perturbations in the dominant singular vector are provided in Tables 4 and 5. These estimates are computed from (Equation 10), which, as noted in Section 3.5, show that the greatest sensitivity will occur when the perturbation heavily weights likelihood parameters  $\theta$  that most affect the posterior and when earthquake parameters have the most uncertainty in the posterior. To estimate the worst-case scenario, we again assume that the perturbation is a 10% relative perturbation along the first singular vector of  $I$ . Among earthquake parameters, the greatest sensitivities for the 1852 event were associated with depth offset (Table 4) because it had the widest distribution according to the posterior measure. Similar calculations are reported in Table 5 for both posterior distributions of the 1820 event.

## 5. Discussion

The results for the 1852 Banda Arc earthquake and tsunami show the promise of the described methodology: Even though the historical accounts of the tsunami are textual in nature and therefore individually prone to much uncertainty, it nevertheless appears that taken together they can be used to determine key characteristics of the causal earthquake. The approach is similar to the “ad hoc” approach described in Liu and Harris (2014), Fisher and Harris (2016) for example, but with a more reproducible and rigorous set of assumptions, a more comprehensive coverage of possible events (the posterior distribution is approximated from hundreds of thousands of samples rather than a handful of particular simulations meant to match the data), and a more clear characterization of uncertainty on the results. The strategy outlined in Section 3.2 can not only readily be applied to any number of historical seismic events but also to any other problem of inverting from textual accounts similar in nature to those described in Section 2 or any other historical or other data that is similarly “small”—sparse and riddled with uncertainty, so long as a reasonably believable forward model is available with parameters on which we can formulate a suitable prior distribution.

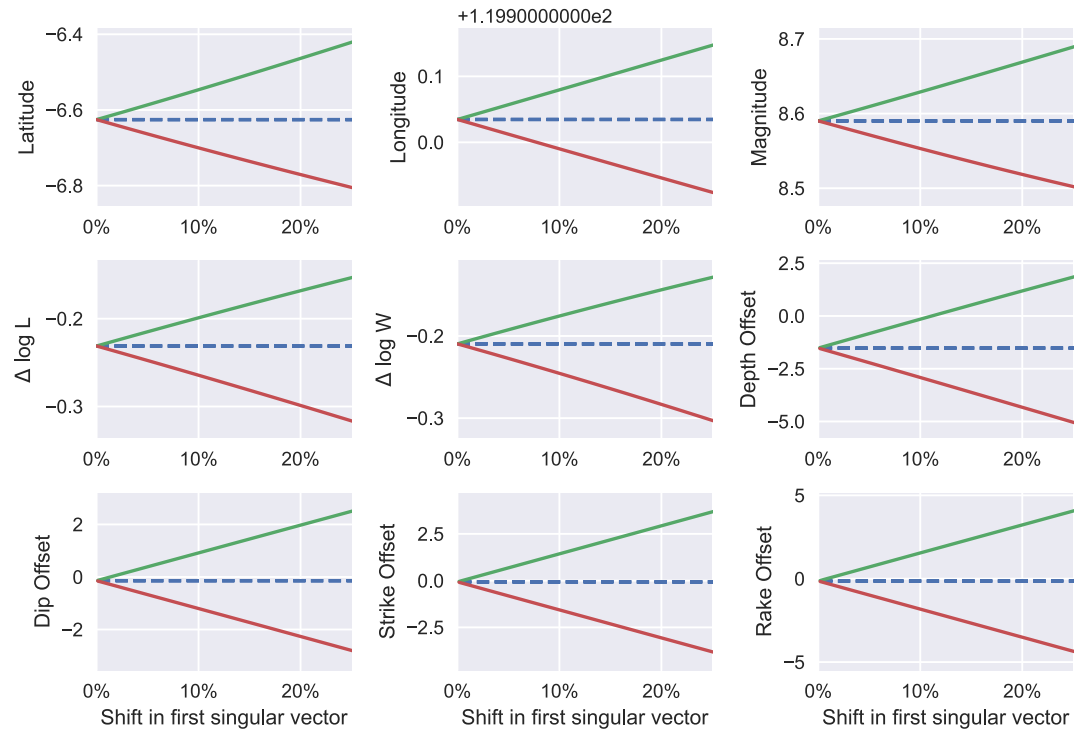


**Figure 7.** Bounds on mean parameter values in terms of relative perturbation in the first singular vector of the Fisher information matrix (see the SV columns of Table 3) for the 1820 Sulawesi event with a Walanae/Selayar earthquake source. Upper and lower bounds are in green and red, respectively. The posterior mean is in blue. The units for these plots are as follows: latitude and longitude (degrees), magnitude (Mw), the  $\Delta$  parameters (log(km)), depth offset (km), and the angular offsets in degrees ( $^{\circ}$ ).

The current study provides formal quantification of some of the uncertainty for this inverse problem and addresses some of the underlying issues in working in the “small data” environment. To be specific, analyzing the numerical approximation of the Hessian near the MAP, and computing the approximate bounds on the sensitivity of the final posterior, give quantifiable measures for analyzing these “small data” problems. The methods outlined here, while applied to the case of historical tsunamigenic earthquakes, are applicable to other settings where the uncertainty in the observable data may be overwhelming. Using these approaches to estimate some of the uncertainty and sensitivity of the setting, we provide justification that the 1852 Banda event was statistically adequately resolved in Ringer et al. (2021). These sensitivity analyses also demonstrate that the seismic source of the 1820 event is very likely from an until very recently undiscovered fault in the Flores Sea.

**Table 4**  
Posterior Variance and Sensitivity Bound According to (Equation 10) by Earthquake Parameter for 1852

Parameter	Variance	Sensitivity bound
Latitude	0.066	0.135
Longitude	0.040	0.105
Magnitude	0.008	0.046
$\Delta \log L$	0.011	0.054
$\Delta \log W$	0.006	0.041
Depth Offset	14.483	1.997

*Note.* Sensitivity bound is for relative perturbation of 10% in the direction of the first (worst-case) singular vector of the Fisher Information matrix.

Although using the numerically approximated Hessian and the approximate bounds on the sensitivity of the posterior provide useful information on the uncertainty in these problems, they do not fully address all of the underlying sensitivity and/or uncertainty. The Hessian approximation we use provides valuable insight into the resolution of the posterior, but only on a local level near the MAP. The approximate bounds on the sensitivity of the posterior are also reliant on sufficiently small perturbations to the posterior so that the higher order terms in (Equation 8) can be neglected, and the choice of the dominant eigenvector to model the most sensitive directions of the posterior, relies on the perturbations being small enough so that nonlinear interactions are less prevalent. Essentially we have focused on the MAP as that is the most pertinent region of the posterior, and we have assumed that our formulation is reasonable enough so that small perturbations are all we need to consider. Despite these limitations, we emphasize that these approaches can be adapted to provide quantifiable estimates on the sensitivity of solutions to “small data”

**Table 5**  
*Posterior Variance and Sensitivity Bound According to (Equation 10) by Earthquake Parameter for the 1820 Sulawesi Event*

Parameter	Flores		Walanae/Selayar	
	Variance	Sensitivity	Variance	Sensitivity
Latitude	0.108557	0.093343	0.108557	0.093343
Longitude	0.402422	0.179718	0.402422	0.179718
Magnitude	0.021577	0.041614	0.021577	0.041614
$\Delta \log L$	0.018109	0.038124	0.018109	0.038124
$\Delta \log W$	0.020772	0.040831	0.020772	0.040831
Depth Offset	0.64787	0.228032	0.64787	0.228032
Dip Offset	13.573413	1.043748	13.573413	1.043748
Strike Offset	8.498352	0.825883	8.498352	0.825883
Rake Offset	22.272118	1.337002	22.272118	1.337002

*Note.* Sensitivity bound is for relative perturbation of 10% in the direction of the first (worst-case) singular vector of the Fisher information matrix.

problems and are far more general than the application of historical seismic events considered here.

In the rest of this section we will discuss the impact of these results on each of the two historical events considered in detail in this study.

### 5.1. Discussion of the 1852 Banda Sea Posterior Distribution

We first observe that the Hessian approximation for the 1852 Banda Sea event depicted in Figure 3 indicates that the posterior is adequately resolved, as all six eigenvalues are clearly negative. From this same computation we see that the steepest concavity near the MAP point follows along the latitude-longitude and magnitude. In particular, the fastest way to decrease the posterior from the MAP point is to select a centroid to the northeast of the MAP and decrease the magnitude, which would lead to a tsunami with wave heights lower than those that match the observational likelihoods as it would place the centroid further from each observation point, and lowering the magnitude would lower the wave height as well.

The sensitive dependence on the arrival times (specifically the means of the observational probability distributions assigned to the arrival times) denoted in Table 2 for the 1852 event is expected as we anticipate that these two arrival times are the dominant observations that triangulate the latitude-longitude location of the centroid, and since there are only two arrival time observations, each one is critical to the inference of the full posterior. The wave height at Ambon is likely emphasized because this particular observation was very precisely specified and so the resultant observational distribution was quite narrow, that is, a small change in the mean would result in a significantly different estimated posterior.

In terms of the actual posterior distribution, the data in Table 4 indicate that depth offset is the least certain inferred parameter for the 1852 event; that is, we have the least amount of confidence on the estimated values of depth offset relative to all other components of the posterior. On the other hand, the small sensitivity for the magnitude,  $\Delta \log L$ , and  $\Delta \log W$  indicate that the inferred values of these three parameters representing the size of the earthquake are quite certain. Hence, we have relatively high confidence in the post-dicted magnitude of the earthquake, and the least confidence in the depth.

### 5.2. Discussion of the 1820 South Sulawesi Earthquake

Turning to the 1820 event, the true MAP point (in the sense of the maximal posterior probability) for the Flores posterior falls near the boundary of the distribution because the preferred geographic location is on the edge of the allowable region prescribed by the prior. That is, our choice of the prior necessarily cuts the distribution off abruptly, but the likelihood prefers the centroid to fall on the edge of this cutoff. This is problematic for the approximation of the Hessian displayed in Figure 4 because there are not a sufficient number of sampled points near this MAP point that allow for an accurate approximation of the Hessian, see Figure 8 which demonstrates the location of the true MAP for both posterior distributions for this event. Instead, we defer to a secondary MAP point that is in the highest density sampled region of the posterior for the calculation presented in the top plots of Figure 4. Hence, this calculation is really an evaluation of the concavity of the posterior in the region of the densest samples, which is actually not the same as the true MAP point for this distribution, indicating that our selected prior distribution was too restrictive in this case, although a more permissive prior distribution would have allowed for earthquakes off of the Flores thrust, which were not considered in the original approach to this problem.

The Hessians of both the Flores and Walanae/Selayar posterior distributions are diagonally dominated with a negative correlation along the diagonal indicating that the different variables are relatively uncorrelated. The dominant eigenvector for the Flores posterior indicates that the easiest route to diminishing the posterior probability is to increase the longitude, that is, move the centroid of the earthquake source to the east. This would not only increase the arrival time of the wave at Sumenep but also pushes the centroid outside the established prior

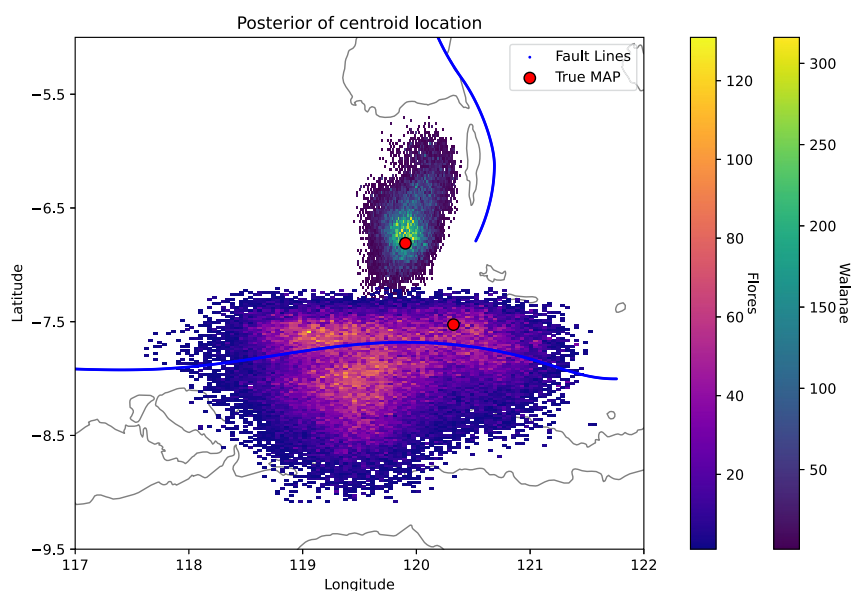


**Figure 8.** A visualization of the posterior distribution on centroid for the 1820 event. The red point specified here is the maximum a posteriori for each posterior, and the color scheme on the point cloud is the frequency of samples (surrogate for the probability).

distribution for the Flores fault and will decrease the likelihood corresponding to the observation at Bima. On the other hand the Walanae/Selayar posterior will optimally decrease by moving the earthquake centroid to the south and decreasing the magnitude, which will yield longer arrival times and wave heights at Bulukumba, which it appears is a critical observation in the construction of the posterior.

Both Hessians for the 1820 event have one eigenvalue that is positive, even though the magnitude of the positive eigenvalue is small in both cases relative to the dominant negative eigenvalue. This is likely due to a combination of numerical error in the Hessian approximation, and a result of the peculiar nature of the prior distributions used to build both of these posteriors. In particular, as noted above and in Paskett et al. (2024) both the Flores and Walanae/Selayar posterior distributions are concentrated on the edge of the prior. The Flores posterior is focused further north than the prior prefers and indeed is on the wrong side of the fault, whereas the Walanae/Selayar posterior is focused on the very southern edge of the fault, once again at the edge of the prior. In particular, the eigenvector corresponding to a positive eigenvalue in the Flores case indicates that an increase in latitude would yield a higher probability, but as the Flores thrust runs primarily east-west, such a movement in the earthquake centroid is not only prohibited by the prior, but is completely unphysical. For the Walanae/Selayar posterior, the eigenvector corresponding to the positive eigenvalue indicates that increasing the magnitude of the earthquake, and marginally moving southeast will increase the probability, but both of these changes are prohibited by the prior distribution and indeed, are not physically feasible earthquake parameters for the Walanae/Selayar fault. Both of these observations indicate that the most likely source of the 1820 Sulawesi tsunami was on neither the Flores thrust nor the Walanae/Selayar faults alone, but may have originated on the previously undiscovered Kalatoa (see Simanjuntak & Ansari, 2023) fault and then triggered somewhere between the two hypothesized sources. Another possibility is the near-simultaneous rupture of a combination of all three faults. This hypothesis arises because the dominant eigenvector of the Hessian for both faults points toward the Kalatoa fault that is beyond the defined boundary of the prior for each possibility as reported here and in Paskett et al. (2024).

The Walanae/Selayar source has a relatively high sensitivity to the specified standard deviation of the arrival time at Bulukumba (value of 0.015 as specified in Table 3) and the specified standard deviation of the wave height at Bulukumba (value of 0.011), but seems to be most sensitive to the specified standard deviation of the wave height at Nipa-Nipa (value of 0.022). This may be because although the Walanae/Selayar source is a closer match to the observations in Bulukumba, it is still not very close to the historical record, with a far lower wave height and an indeterminate arrival time. A possible interpretation for the higher sensitivity for the observation at Nipa-Nipa is



that Nipa-Nipa and Bulukumba are not geographically very far apart yet the historical record indicated a vastly different wave height between the two locations, which does not appear to be supported by the simulations reported here. The Walanae/Selayar source does not appear to be sensitive to the recorded arrival time at Sumenep, indicating that the posterior seems to have adequately balanced the differences between the prior and likelihood for this observation unlike the case of the Flores source for this event. As shown in Table 3 the most sensitive parameter for the Flores source is the standard deviation of the wave height at Bulukumba, which likely indicates that the specified source cannot adequately capture the variation in the wave heights at this location without significantly modifying the observational probability distribution here.

The most significant changes to the posterior distribution for both sources appears to be making smaller waves at Bulukumba less plausible (push the mean up and the standard deviation down) and making large waves at Nipa-Nipa more plausible (increase both mean and standard deviation). As noted above, this is because these two observation points are geographically close, yet the reported wave height at Nipa-Nipa is much smaller than that reported at Bulukumba. As a result, the most likely change in the observational probabilities to match the simulations would be to put these two observations more in line with each other.

Variance and sensitivity bounds for the 1820 event (Table 5) indicate that the inference did not provide much information about the value of the dip, strike, and rake offset parameters, whereas parameters related to earthquake size and location were more constrained and robust to changes in the likelihood parameters. Essentially the posterior distribution provides a reasonable post-diction on earthquake magnitude and centroid location whereas the other geometric aspects of the fault are far less constrained by the historical tsunamigenic record.

## 6. Conclusions

We have reviewed an approach to Bayesian inference that incorporates non-additive uncertainty into the inverse problem using data augmentation. A special case of this approach was used on the problem of inferring the earthquake parameters for causal earthquakes that generated historical tsunamis in the Indonesian archipelago relying on sparse and uncertain observational data. The results obtained demonstrate that the Bayesian framework and statistical approach can be used to make significant progress on problems of this type where the data are “small”.

We further identify the utility of this approach by incorporating specific methods that analyze the sensitivity of the Bayesian approach to this problem. Using a numerical approximation of the Hessian near the MAP, and approximate sensitivity bounds on the posterior itself, we identify some of the limitations of this Bayesian approach to these seismic problems. This sensitivity analysis is presented in a general enough fashion that adaptation to other settings where the data are sparse and uncertain are feasible, that is, we have described initial steps that can be taken to validate the Bayesian solution to “small data” inverse problems. For the application at hand, we have shown that the posterior distribution for the 1852 Banda Sea earthquake is fully resolved. These same methods also give indication that the 1820 tsunami in the Flores Sea was most probably caused by an earthquake source along the newly discovered Kalatua fault, or perhaps even according to a multi-rupture scenario akin to the 2023 dual rupture in Turkey or the 2016 Kaikoura rupture in New Zealand. All of these results emphasize the need to include such statistical, probabilistic, and numerical estimators/bounds in any discussion of such problems where the uncertainty is high.

## Appendix A: Derivation of the Fisher Information Matrix

In this appendix we derive the FIM  $\mathcal{I}$  associated with the parameterization of the posterior measure given in (Equation 1). The FIM associated with parameter  $\theta$  is given by

$$\mathcal{I}(P^{(\theta)}) = \int \nabla_{\theta} \log p^{(\theta)}(\mathbf{u}) (\nabla_{\theta} \log p^{(\theta)}(\mathbf{u}))^T P^{(\theta)}(d\mathbf{u}) \quad (\text{A1})$$

where  $P^{(\theta)}$  is the posterior measure and  $p^{(\theta)}$  its associated density given by (see Equations 1 and 4)

$$p_{\text{post}}^{(\theta)}(\mathbf{u}|\mathbf{y})d\mathbf{u} = \frac{1}{Z^{(\theta)}} p_0^{(\theta)}(\mathbf{u}) p(\mathbf{y}|\mathcal{G}(\mathbf{u})) d\mathbf{u},$$

where we have used the likelihood specified as  $p(\mathbf{y}|\mathcal{G}(\mathbf{u}))$ . Since the focus of this paper is on modeling of historical observations via observation distributions, we will focus on the case where  $\theta$  describes the observation distributions, that is,  $\theta$  are the parameters used to define the distributions  $p_0^{(\theta)}(\mathbf{u}|\mathbf{y})$  and  $p(\mathbf{y}|\mathcal{G}(\mathbf{u}))$ . In this case, we have

$$\mathcal{I}_{ij}(P^{(\theta)}) = \text{Cov}_{P^{(\theta)}} \left[ \frac{\partial}{\partial \theta_i} \Phi^{(\theta)}, \frac{\partial}{\partial \theta_j} \Phi^{(\theta)} \right]$$

where  $\text{Cov}_{P^{(\theta)}}$  is the covariance according to the posterior and  $\Phi^{(\theta)}$  is the negative log-likelihood given by

$$\Phi^{(\theta)}(\mathbf{u}) := -\log p(\mathbf{y}|\mathcal{G}(\mathbf{u})),$$

where we have suppressed the dependence on the observed data  $\mathbf{y}$  to simplify the notation below. Thus, to compute the FIM, we compute the derivative of  $\Phi^{(\theta)}$  with respect to each observation parameter (the “score”) and then compute the covariance of each pair of scores, which we approximate using the observations associated with the approximate posterior samples. Since the individual distributions making up  $p(\mathbf{y}|\mathcal{G}(\mathbf{u}))$  are assumed to be independent, the derivatives can be computed separately for each observation distribution. We now consider each type of observation distribution used to construct the posterior distributions in this article.

### A1. Normal Distribution

For a normal distribution with mean  $\mu$  and standard deviation  $\sigma$ , we have the following:

$$\Phi^{(\theta)}(x) = \frac{1}{2\sigma^2}[\mathcal{G}(\mathbf{u}) - \mu]^2 + \ln \sigma + \frac{1}{2}\ln(2\pi)$$

Then the derivatives with respect to parameters  $\mu$  and  $\sigma$  are given by:

$$\begin{aligned} \frac{\partial}{\partial \mu} \Phi^{(\theta)}(\mathbf{u}) &= -\frac{1}{\sigma^2}[\mathcal{G}(\mathbf{u}) - \mu] \\ \frac{\partial}{\partial \sigma} \Phi^{(\theta)}(\mathbf{u}) &= -\frac{1}{\sigma^3}[\mathcal{G}(\mathbf{u}) - \mu]^2 + \frac{1}{\sigma}. \end{aligned}$$

### A2. Skew-Norm Distribution

For a skew-normal distribution with location  $\mu$ , scale  $\sigma$ , and skew  $a$ , we have the following:

$$\Phi(\mathbf{u}) = \frac{1}{2}\tilde{x}(\mathbf{u})^2 + \ln \sigma + \frac{1}{2}\ln(2\pi) - \ln[1 + \text{erf}(z(\mathbf{u}))]$$

where  $\text{erf}$  is the error function and  $\tilde{x}, z$  are given by

$$\tilde{x}(\mathbf{u}) := \frac{\mathcal{G}(\mathbf{u}) - \mu}{\sigma} \quad \text{and} \quad z(\mathbf{u}) := \frac{a\tilde{x}(\mathbf{u})}{\sqrt{2}}.$$

Then the derivative with respect to  $z$  and  $\tilde{x}$  are given by

$$\begin{aligned} \frac{\partial}{\partial z} \Phi(\mathbf{u}) &= -\frac{2}{\sqrt{\pi}} \frac{e^{-z(\mathbf{u})^2}}{1 + \text{erf}(z(\mathbf{u}))} \\ \frac{\partial}{\partial \tilde{x}} \Phi(\mathbf{u}) &= \frac{\partial}{\partial \tilde{x}} \Phi(\mathbf{u}) + \frac{\partial \Phi}{\partial z}(\mathbf{u}) \frac{\partial z}{\partial \tilde{x}}(\mathbf{u}) = \tilde{x}(\mathbf{u}) - \sqrt{\frac{2}{\pi}} a \frac{e^{-z(\mathbf{u})^2}}{1 + \text{erf}(z(\mathbf{u}))}, \end{aligned}$$

so that the derivatives with respect to parameters  $a, \mu$ , and  $\sigma$  are

$$\begin{aligned}\frac{\partial}{\partial a}\Phi(\mathbf{u}) &= \frac{\partial\Phi}{\partial z}(\mathbf{u})\frac{\partial z}{\partial a}(\mathbf{u}) = -\sqrt{\frac{2}{\pi}}\tilde{x}(\mathbf{u})\frac{e^{-z(\mathbf{u})^2}}{1+\operatorname{erf}(z(\mathbf{u}))} \\ \frac{\partial}{\partial\mu}\Phi(\mathbf{u}) &= \frac{\partial\Phi}{\partial\tilde{x}}(\mathbf{u})\frac{\partial\tilde{x}}{\partial\mu}(\mathbf{u}) = -\frac{1}{\sigma}\left[\tilde{x}(\mathbf{u}) - \sqrt{\frac{2}{\pi}}a\frac{e^{-z(\mathbf{u})^2}}{1+\operatorname{erf}(z(\mathbf{u}))}\right] \\ \frac{\partial}{\partial\sigma}\Phi(\mathbf{u}) &= \frac{\partial}{\partial\sigma}\Phi(\mathbf{u}) + \frac{\partial\Phi}{\partial\tilde{x}}(\mathbf{u})\frac{\partial\tilde{x}}{\partial\sigma}(\mathbf{u}) = \frac{1}{\sigma}\left[1 - \tilde{x}(\mathbf{u})^2 + \frac{2z(\mathbf{u})}{\sqrt{\pi}}\frac{e^{-z(\mathbf{u})^2}}{1+\operatorname{erf}(z(\mathbf{u}))}\right].\end{aligned}$$

### A3. Chi Distribution

For the Chi distribution with location  $\mu$ , scale  $\sigma$ , and degrees of freedom  $k$ , we have

$$\Phi(\mathbf{u}) = \frac{1}{2}\tilde{x}(\mathbf{u})^2 + \ln \sigma + \left(\frac{k}{2} - 1\right) \ln 2 + \ln \Gamma(k/2) - (k-1) \ln \tilde{x}(\mathbf{u}),$$

where  $\Gamma$  is the gamma function and  $\tilde{x}$  is given by

$$\tilde{x}(\mathbf{u}) := \frac{G_t(\mathbf{u}) - \mu}{\sigma}.$$

The derivative with respect to  $\tilde{x}$  is given by

$$\frac{\partial\Phi}{\partial\tilde{x}}(\mathbf{u}) = \tilde{x}(\mathbf{u}) - (k-1)\tilde{x}(\mathbf{u})^{-1}.$$

Then the derivatives with respect to parameters  $\mu$ ,  $\sigma$ , and  $k$  are given by

$$\begin{aligned}\frac{\partial\Phi}{\partial\mu}(\mathbf{u}) &= \frac{\partial\Phi}{\partial\tilde{x}}\frac{\partial\tilde{x}}{\partial\mu} = -\frac{1}{\sigma}(\tilde{x}(\mathbf{u}) - (k-1)\tilde{x}(\mathbf{u})^{-1}) \\ \frac{\partial\Phi}{\partial\sigma}(\mathbf{u}) &= \frac{\partial\Phi}{\partial\sigma} + \frac{\partial\Phi}{\partial\tilde{x}}\frac{\partial\tilde{x}}{\partial\sigma} = -\frac{1}{\sigma}(\tilde{x}(\mathbf{u})^2 - k). \\ \frac{\partial\Phi}{\partial k}(\mathbf{u}) &= \frac{1}{2}\ln 2 + \frac{1}{2}\psi(k/2) - \ln \tilde{x}(\mathbf{u})\end{aligned}$$

where  $\psi$  is the digamma function.

## Appendix B: Derivation of Bounds in Terms of Relative Entropy

In this section, we derive from (Equation 9) more explicit bounds on  $\mathbb{E}_Q[f]$ —first in terms of  $\mathcal{R}(Q||P)$  and then independent of  $\mathcal{R}(Q||P)$ . These bounds were used to generate Figure B1, below, which shows the bounds on estimates of parameters of the 1852 Banda Arc earthquake in terms of  $\mathcal{R}(Q||P)$ . These bounds are then combined with the estimate from (Equation 8) to produce bounds in terms of relative parameter value changes.

### B1. Optimal Bound for a Given $\mathcal{R}(Q||P)$

Here we derive a relationship between the relative entropy  $\mathcal{R}(Q||P)$  and  $c < \infty$  for which the bounds given by (Equation 9) are achieved. We first assume that such a  $c$  exists; the case where the supremum/infimum are achieved as  $c \rightarrow \infty$  is discussed in the next subsection. Denoting  $\tilde{f} = f - \mathbb{E}_P[f]$  and differentiating the right hand side of (Equation 9) with respect to  $c$  and setting the corresponding value equal to zero yields that the infimum of the upper bound is achieved when  $c$  satisfies

$$\mathcal{R}(Q||P) = c \frac{\mathbb{E}_P[\tilde{f}e^{c\tilde{f}}]}{\mathbb{E}_P[e^{c\tilde{f}}]} - \log \mathbb{E}_P[e^{c\tilde{f}}] = c \frac{E_2(f, c)}{E_1(f, c)} - \log E_1(f, c) \quad (\text{B1})$$

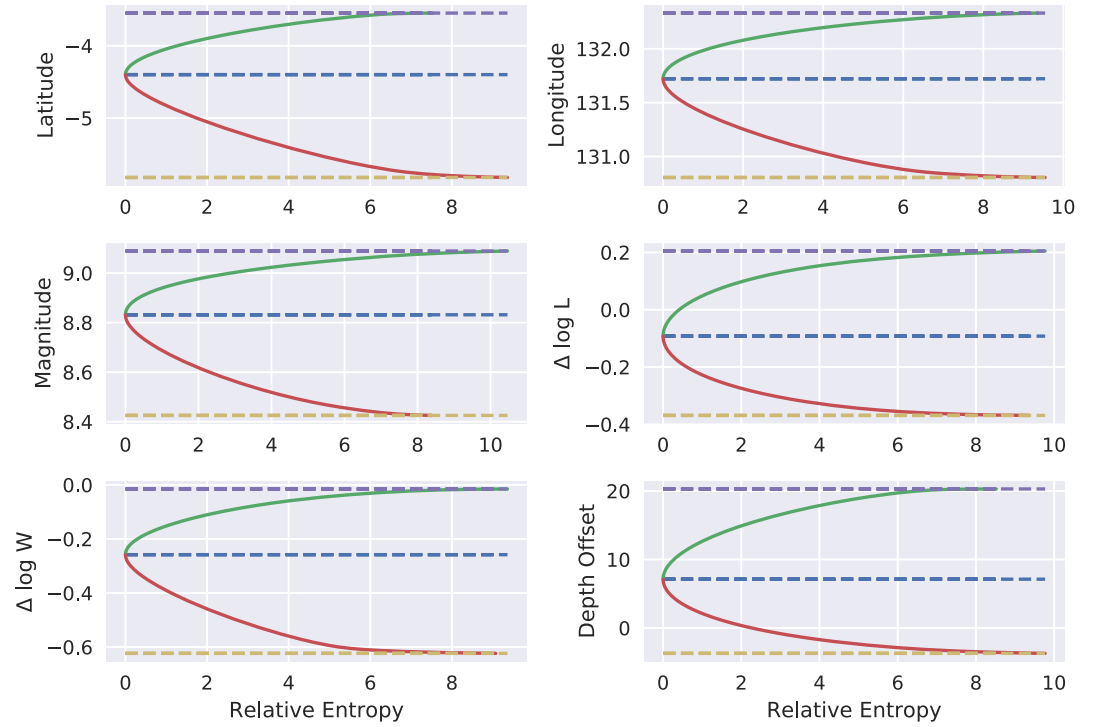


**Figure B1.** Bounds on mean parameter values by relative entropy from the computed posterior for the 1852 Banda Sea event. Upper and lower bounds are in green and red, respectively. The posterior mean is in blue and the estimated uniform upper and lower bounds are in purple and yellow, respectively. The units for these plots are as follows: latitude and longitude (degrees), magnitude (Mw), the  $\Delta$  parameters (log(km)), and depth offset (km).

and similarly for the lower bound  $c$  must satisfy

$$\mathcal{R}(Q||P) = -c \frac{\mathbb{E}_P[\tilde{f}e^{-c\tilde{f}}]}{\mathbb{E}_P[e^{-c\tilde{f}}]} - \log \mathbb{E}_P[e^{-c\tilde{f}}] = -c \frac{E_2(f, -c)}{E_1(f, -c)} - \log E_1(f, -c), \quad (\text{B2})$$

where to simplify notation we have defined

$$E_1(f, c) = \mathbb{E}_P[e^{c\tilde{f}}] \quad \text{and} \quad E_2(f, c) = \mathbb{E}_P[\tilde{f}e^{c\tilde{f}}].$$

Denoting the  $c$  achieving these upper and lower bounds by  $c_+$  and  $c_-$ , respectively, and plugging these values back into (Equation 9) yields the bounds

$$\frac{E_2(f, -c_-)}{E_1(f, -c_-)} \leq \mathbb{E}_Q[f] - \mathbb{E}_P[f] \leq \frac{E_2(f, c_+)}{E_1(f, c_+)}. \quad (\text{B3})$$

It is not clear how to invert (Equations B1 and B2) to find the optimal  $c$  for a given  $\mathcal{R}(Q||P)$ , so to generate Figure B1 we generate a list of  $c$  values, plug them into (Equation B1) to find the  $\mathcal{R}(Q||P)$  for which they achieve the optimal upper bound and into (Equation B3) to compute the associated upper bounds (analogously for the lower bounds), and plot those values against each other.

## B2. Bounds Independent of $\mathcal{R}(Q||P)$

In this section, we consider the case where the bounds in (Equation 9) are achieved as  $c \rightarrow \infty$ , that is, are independent of  $\mathcal{R}(Q||P)$ . From (Equation 9), we have for any  $Q \ll P$

$$\mathbb{E}_Q[f] - \mathbb{E}_P[f] \leq \sup_{c>0} \frac{1}{c} \log \mathbb{E}_P[e^{c(f-\mathbb{E}_P[f])}] + \frac{1}{c} \mathcal{R}(Q||P).$$

Then clearly if

$$U := \lim_{c \rightarrow \infty} \frac{1}{c} \log \mathbb{E}_P[e^{c(f-\mathbb{E}_P[f])}] < \infty, \quad (\text{B4})$$

then for any  $Q \ll P$  we have

$$\mathbb{E}_Q[f] - \mathbb{E}_P[f] \leq \lim_{c \rightarrow \infty} \left\{ \frac{1}{c} \log \mathbb{E}_P[e^{c(f-\mathbb{E}_P[f])}] + \frac{1}{c} \mathcal{R}(Q||P) \right\} = U.$$

Finally, we note that since the logarithm and exponential are continuous, we have the following:

$$\begin{aligned} U &= \lim_{c \rightarrow \infty} \frac{1}{c} \log \mathbb{E}_P[e^{c(f-\mathbb{E}_P[f])}] = \lim_{c \rightarrow \infty} \log(\mathbb{E}_P[e^{c(f-\mathbb{E}_P[f])}])^{1/c} \\ &= \log \lim_{c \rightarrow \infty} (\mathbb{E}_P[e^{c(f-\mathbb{E}_P[f])}])^{1/c} = \log \|e^{f-\mathbb{E}_P[f]}\|_{\infty} = \sup \text{ess}_P[f] - \mathbb{E}_P[f] \end{aligned}$$

An analogous relationship will hold for the lower bound. Thus if  $f$  is an essentially bounded random variable according to  $P$ , we have the following bound for any  $Q \ll P$ :

$$\inf \text{ess}_P[f] \leq \mathbb{E}_Q[f] \leq \sup \text{ess}_P[f].$$

Figure B2.

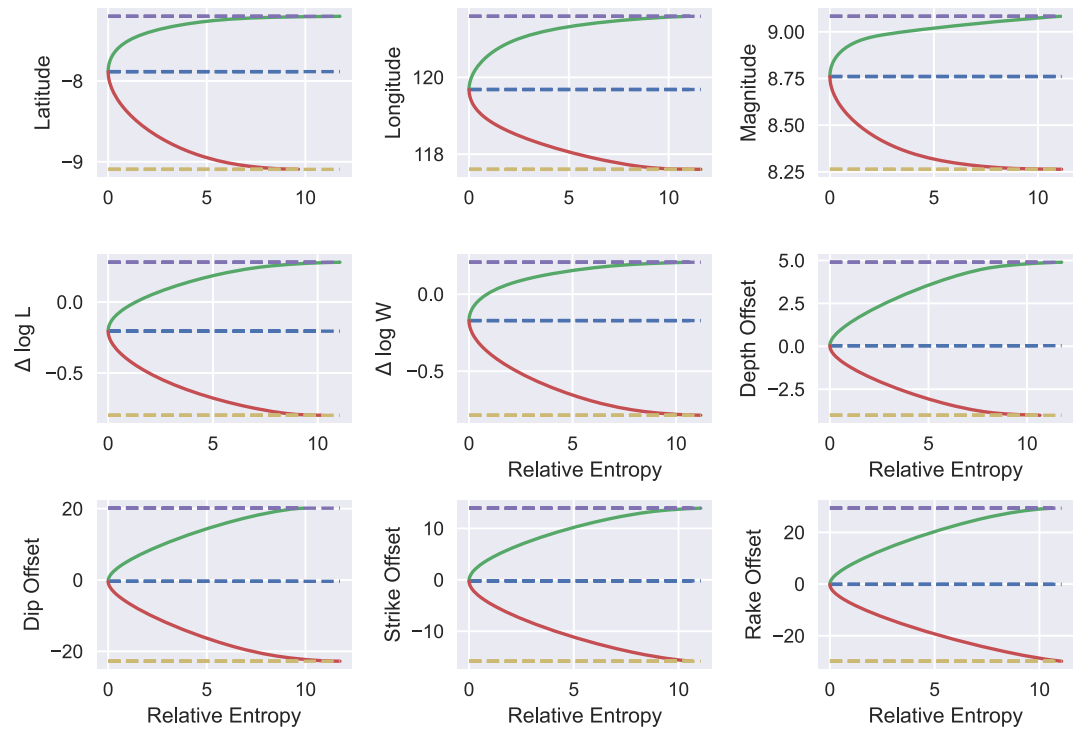


**Figure B2.** Bounds on mean parameter values by relative entropy from computed posterior for the 1820 Flores hypothesis. Upper and lower bounds are in green and red, respectively. The posterior mean is in blue and the estimated uniform upper and lower bounds are in purple and yellow, respectively. The units for these plots are as follows: latitude and longitude (degrees), magnitude (Mw), the  $\Delta$  parameters (log(km)), depth offset (km), and the angular offsets in degrees ( $^{\circ}$ ).



Figure B3.

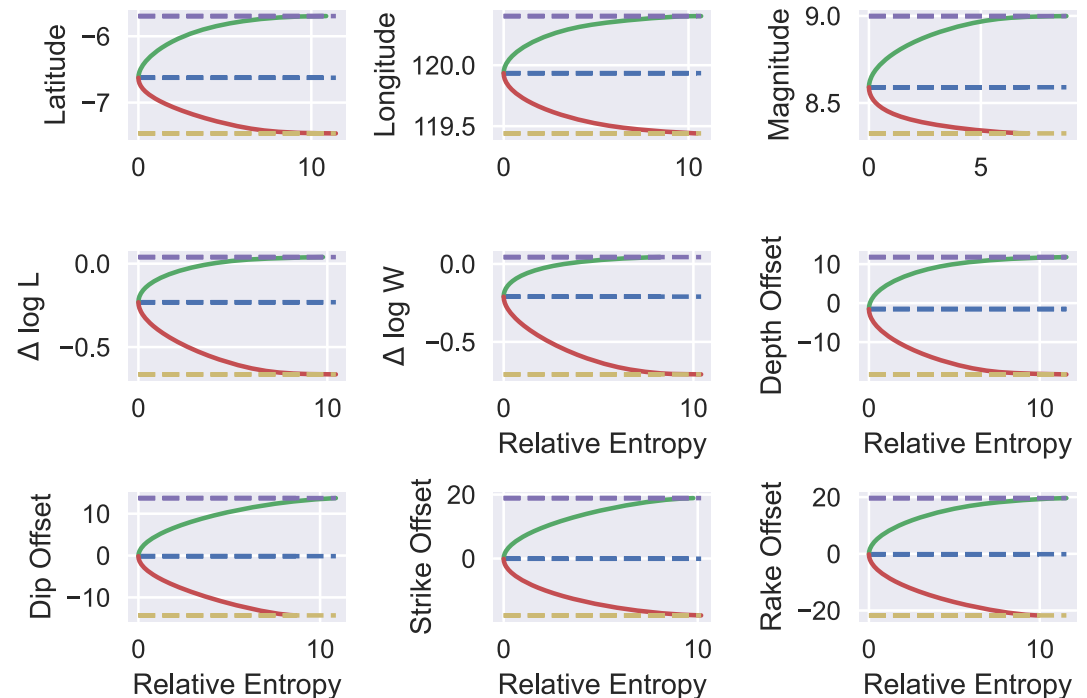


**Figure B3.** Bounds on mean parameter values by relative entropy from computed posterior for the 1820 Walanae/Selayar fault hypothesis. Upper and lower bounds are in green and red, respectively. The posterior mean is in blue and the estimated uniform upper and lower bounds are in purple and yellow, respectively. The units for these plots are as follows: latitude and longitude (degrees), magnitude (Mw), the  $\Delta$  parameters (log(km)), depth offset (km), and the angular offsets in degrees ( $^{\circ}$ ).

### Conflict of Interest

The authors declare no conflicts of interest relevant to this study.

### Data Availability Statement

All the analysis performed for this article is contained in the repository at [http://github.com/jpw37/tsunami\\_methods](http://github.com/jpw37/tsunami_methods), see also Whitehead (2025) for the specific release used in this article. In particular, the Jupyter notebooks (Python) used to create all of the Tables and Figures in this article are included there. The data required to generate the analysis and figures contained here are also included in this repository.

### References

- Albert, J. H., & Chib, S. (1993). Bayesian analysis of binary and polychotomous response data. *Journal of the American Statistical Association*, 88(422), 669–679. <https://doi.org/10.1080/01621459.1993.10476321>
- Arrowsmith, S. J., Trugman, D. T., MacCarthy, J., Bergen, K. J., Lumley, D., & Magnani, M. B. (2022). Big data seismology. *Reviews of Geophysics*, 60(2), e2021RG000769. <https://doi.org/10.1029/2021rg000769>
- Bakun, W. (2002). USGS earthquake magnitude working group [Computer Software Manual]. Retrieved from <https://earthquake.usgs.gov/data/comcat/catalog/official/>
- Berger, M. J., George, D. L., LeVeque, R. J., & Mandli, K. T. (2011). The GeoClaw software for depth-averaged flows with adaptive refinement. *Advances in Water Resources*, 34(9), 1195–1206. <https://doi.org/10.1016/j.advwatres.2011.02.016>
- Bergsma, P. (1868). Aardbevingen in den indischen archipel gedurende het Jaar 1867. *Natuurkundig Tijdschrift Voor Nederlandsch-Indië*, 30, 478–485.
- Bryant, E., Walsh, G., & Abbott, D. (2007). Cosmogenic mega-tsunami in the Australia region: Are they supported by Aboriginal and Maori legends? *Geological Society, London, Special Publications*, 273(1), 203–214. <https://doi.org/10.1144/gsl.sp.2007.273.01.16>
- Bui-Thanh, T., Ghattas, O., Martin, J., & Stadler, G. (2013). A computational framework for infinite-dimensional Bayesian inverse problems part I: The linearized case, with application to global seismic inversion. *SIAM Journal on Scientific Computing*, 35(6), A2494–A2523. <https://doi.org/10.1137/12089586x>
- Butler, T., Estep, D., Tavener, S., Dawson, C., & Westerink, J. J. (2014). A measure-theoretic computational method for inverse sensitivity problems III: Multiple quantities of interest. *SIAM/ASA Journal on Uncertainty Quantification*, 2(1), 174–202. <https://doi.org/10.1137/130930406>

### Acknowledgments

The authors acknowledge the Office Research Computing at BYU (<http://rc.byu.edu>) and Advanced Research Computing at Virginia Tech (<http://www.arc.vt.edu>) for providing computational resources and technical support that have contributed to the results reported within this paper. We also thank G. Simpson for pointing us toward the theoretical results that ultimately yielded Section 3.5; J. Guinness and R. Gramacy for helpful feedback on an early presentation of this work; as well as C. Ashcraft, A. Avery, J. Callahan, G. Carver, J. Fullwood, S. Giddens, M. Harward, R. Hilton, C. Kesler, M. H. Klein, K. Lighthouse, M. Morrise, C. Noorda, A. Robertson, T. Paskett, P. Smith, D. Stewart, R. Wonnacott, and many other students at BYU who participated in the setup of the inverse problem for the events discussed here. We also acknowledge the valuable contribution of several reviewers whose comments have greatly improved the manuscript. JAK was partially supported by NSF Grant DMS-2108791. JPW was partially supported by the Simons Foundation travel Grant under 586788 as well as by NSF Grants DMS-2206762 and CCF-2343286. NEGH was partially supported by NSF Grants DMS-1816551 and DMS-2108790. AJH was supported by NIH Grant K25 AI153816 and NSF Grants DMS 2152774 and DMS 2236854. JPW and RH would like to thank the Office of Research and Creative Activities at BYU for supporting several of the students' efforts on this project through a Mentoring Environment Grant, as well as generous support from the College of Physical and Mathematical Sciences and the Mathematics and Geology Departments. We also acknowledge the visionary support of Geoscientists Without Borders.

- Butler, T., & Hakula, H. (2020). What do we hear from a drum? A data-consistent approach to quantifying irreducible uncertainty on model inputs by extracting information from correlated model output data. *Computer Methods in Applied Mechanics and Engineering*, 370, 113228. <https://doi.org/10.1016/j.cma.2020.113228>
- Butler, T., Jakeman, J., & Wildey, T. (2018). Combining push-forward measures and Bayes' rule to construct consistent solutions to stochastic inverse problems. *SIAM Journal on Scientific Computing*, 40(2), A984–A1011. <https://doi.org/10.1137/16m1087229>
- Butler, T., Wildey, T., & Yen, T. Y. (2020). Data-consistent inversion for stochastic input-to-output maps. *Inverse Problems*, 36(8), 085015. <https://doi.org/10.1088/1361-6420/ab8f83>
- Casella, G., & Berger, R. L. (2021). *Statistical inference*. Cengage Learning.
- Cummins, P. R., Pranantyo, I. R., Pownall, J. M., Griffin, J. D., Meilano, I., & Zhao, S. (2020). Earthquakes and tsunamis caused by low-angle normal faulting in the Banda Sea, Indonesia. *Nature Geoscience*, 13(4), 312–318. <https://doi.org/10.1038/s41561-020-0545-x>
- Dashti, M., & Stuart, A. M. (2017). The Bayesian approach to inverse problems. *Handbook of Uncertainty Quantification*, 311–428. [https://doi.org/10.1007/978-3-319-12385-1\\_7](https://doi.org/10.1007/978-3-319-12385-1_7)
- del Castillo-Negrete, C., Spence, R., Butler, T., & Dawson, C. (2024). Sequential maximal updated density parameter estimation for dynamical systems with parameter drift. *arXiv preprint arXiv:2405.08307*.
- del Villar, A. M. (2004). 19th century earthquakes in Mexico: Three cases, three comparative studies. *Annals of Geophysics*, 47(2–3).
- Doucet, A., De Freitas, N., & Gordon, N. (2001). *Sequential Monte Carlo methods in practice*. Springer. <https://doi.org/10.1007/978-1-4757-3437-9>
- Dupuis, P., Katsoulakis, M. A., Pantazis, Y., & Plecháč, P. (2016). Path-space information bounds for uncertainty quantification and sensitivity analysis of stochastic dynamics. *SIAM/ASA Journal on Uncertainty Quantification*, 4(1), 80–111. <https://doi.org/10.1137/15m1025645>
- Fisher, R. A. (1922). On the mathematical foundations of theoretical statistics. *Philosophical Transactions of the Royal Society of London—Series A: Containing Papers of a Mathematical or Physical Character* (Vol. 222(594–604), pp. 309–368).
- Fisher, T. L., & Harris, R. A. (2016). Reconstruction of 1852 Banda Arc megathrust earthquake and tsunami. *Natural Hazards*, 83(1), 667–689. <https://doi.org/10.1007/s11069-016-2345-6>
- Gagan, M. K., Sosdian, S. M., Scott-Gagan, H., Sieh, K., Hantoro, W. S., Natawidjaja, D. H., et al. (2015). Coral 13c/12c records of vertical seafloor displacement during megathrust earthquakes west of Sumatra. *Earth and Planetary Science Letters*, 432, 461–471. <https://doi.org/10.1016/j.epsl.2015.10.002>
- Gelman, A., Carlin, J. B., Stern, H. S., & Rubin, D. B. (2014). *Bayesian data analysis* (Vol. 2). Taylor and Francis.
- Gelman, A., Rubin, D. B., et al. (1992). Inference from iterative simulation using multiple sequences. *Statistical Science*, 7(4), 457–472. <https://doi.org/10.1214/ss/1177011136>
- Giraldi, L., Le Maître, O. P., Mandli, K. T., Dawson, C. N., Hoteit, I., & Knio, O. M. (2017). Bayesian inference of earthquake parameters from buoy data using a polynomial chaos-based surrogate. *Computational Geosciences*, 21(4), 683–699. <https://doi.org/10.1007/s10596-017-9646-z>
- Goldfinger, C., Nelson, C. H., Johnson, J. E., & Party, S. S. (2003). Holocene earthquake records from the Cascadia subduction zone and northern San Andreas fault based on precise dating of offshore turbidites. *Annual Review of Earth and Planetary Sciences*, 31(1), 555–577. <https://doi.org/10.1146/annurev.earth.31.100901.141246>
- González, F. I., LeVeque, R. J., Chamberlain, P., Hirai, B., Varkovitzky, J., & George, D. L. (2011). Validation of the geoclaw model. In *NTHMP MMS tsunami inundation model validation workshop. GeoClaw tsunami modeling group*.
- Griffin, J., Nguyen, N., Cummins, P., & Cipta, A. (2018). Historical earthquakes of the eastern sunda arc: Source mechanisms and intensity-based testing of Indonesia's National seismic hazard assessment. *Bulletin of the Seismological Society of America*, 109(1), 43–65. <https://doi.org/10.1785/0120180085>
- Gutenberg, B., & Richter, C. (1955). Magnitude and energy of earthquakes. *Nature*, 176(4486), 795–795. <https://doi.org/10.1038/176795a0>
- Gutenberg, B., & Richter, C. F. (1956). Earthquake magnitude, intensity, energy, and acceleration: (second paper). *Bulletin of the Seismological Society of America*, 46(2), 105–145. <https://doi.org/10.1785/bssa0460020105>
- Harris, R. A., & Major, J. (2016). *Waves of destruction in the east Indies: The Wichmann catalogue of earthquakes and tsunami in the Indonesian region from 1538 to 1877*. (Vol. 441(1), pp. SP441–SP442). Geological Society, London, Special Publications. <https://doi.org/10.1144/sp441.2>
- Hayes, G. P., Moore, G. L., Portner, D. E., Hearne, M., Flamme, H., Furtney, M., & Smoczyk, G. M. (2018). Slab2, a comprehensive subduction zone geometry model. *Science*, 362(6410), 58–61. <https://doi.org/10.1126/science.aat4723>
- Helton, J., Johnson, J., Sallaberry, C., & Storlie, C. (2006). Survey of sampling-based methods for uncertainty and sensitivity analysis. *Reliability Engineering and System Safety*, 91(10), 1175–1209. <https://doi.org/10.1016/j.res.2005.11.017>
- Holbrook, A. J., Ji, X., & Suchard, M. A. (2022). Bayesian mitigation of spatial coarsening for a Hawkes model applied to gunfire, wildfire and viral contagion. *Annals of Applied Statistics*, 16(1), 573–595. <https://doi.org/10.1214/21-AOAS1517>
- Jankaew, K., Atwater, B. F., Sawai, Y., Choowong, M., Charoentitrat, T., Martin, M. E., & Prendergast, A. (2008). Medieval forewarning of the 2004 Indian Ocean tsunami in Thailand. *Nature*, 455(7217), 1228–1231. <https://doi.org/10.1038/nature07373>
- Kaipio, J., & Somersalo, E. (2005). *Statistical and computational inverse problems* (Vol. 160). Springer Science and Business Media.
- Kong, Q., Trugman, D. T., Ross, Z. E., Bianco, M. J., Meade, B. J., & Gerstoft, P. (2019). Machine learning in seismology: Turning data into insights. *Seismological Research Letters*, 90(1), 3–14. <https://doi.org/10.1785/0220180259>
- Kovach, R. L., & Kovach, R. L. (2004). *Early earthquakes of the Americas*. Cambridge University Press.
- LeVeque, R. J., George, D. L., & Berger, M. J. (2011). Tsunami modelling with adaptively refined finite volume methods. *Acta Numerica*, 20, 211–289. <https://doi.org/10.1017/S0962492911000043>
- LeVeque, R. J., & George, D. L. (2008). High-resolution finite volume methods for the shallow water equations with bathymetry and dry states. In *Advanced numerical models for simulating tsunami waves and runup* (pp. 43–73). World Scientific.
- Liu, Z. Y. C., & Harris, R. A. (2014). Discovery of possible mega-thrust earthquake along the Seram Trough from records of 1629 tsunami in eastern Indonesian region. *Natural Hazards*, 72(3), 1311–1328. <https://doi.org/10.1007/s11069-013-0597-y>
- Mannakee, B. K., Ragsdale, A. P., Transtrum, M. K., & Gutenkunst, R. N. (2016). Sloppiness and the geometry of parameter space. In L. Geris & D. Gomez-Cabrero (Eds.), *Uncertainty in biology: A computational modeling approach* (pp. 271–299). Springer International Publishing. [https://doi.org/10.1007/978-3-319-21296-8\\_11](https://doi.org/10.1007/978-3-319-21296-8_11)
- Martin, J., Wilcox, L. C., Burstedde, C., & Ghattas, O. (2012). A stochastic newton MCMC method for large-scale statistical inverse problems with application to seismic inversion. *SIAM Journal on Scientific Computing*, 34(3), A1460–A1487. <https://doi.org/10.1137/110845598>
- Martin, S. S., Cummins, P. R., & Meltzner, A. J. (2022). Gempa Nusantara: A database of 7380 macroseismic observations for 1200 historical earthquakes in Indonesia from 1546 to 1950. *Bulletin of the Seismological Society of America*, 112(6), 2958–2980. <https://doi.org/10.1785/0120220047>

- Martin, S. S., Li, L., Okal, E. A., Morin, J., Tetteroo, A. E. G., Switzer, A. D., & Sieh, K. E. (2019). Reassessment of the 1907 Sumatra "Tsunami Earthquake" based on macroseismic, seismological, and tsunami observations, and modeling. *Pure and Applied Geophysics*, 176(7), 2831–2868. <https://doi.org/10.1007/s00024-019-02134-2>
- McClarren, R. G. (2018). Regression approximations to estimate sensitivities. In *Uncertainty quantification and predictive computational science: A foundation for physical scientists and engineers* (pp. 111–128). Springer International Publishing. [https://doi.org/10.1007/978-3-319-99525-0\\_5](https://doi.org/10.1007/978-3-319-99525-0_5)
- Meltzner, A. J., Sieh, K., Chiang, H.-W., Shen, C.-C., Suwargadi, B. W., Natawidjaja, D. H., et al. (2010). Coral evidence for earthquake recurrence and an AD 1390–1455 cluster at the south end of the 2004 Aceh–Andaman rupture. *Journal of Geophysical Research*, 115(B10). <https://doi.org/10.1029/2010jb007499>
- Minoura, K., Imamura, F., Sugawara, D., Kono, Y., & Iwashita, T. (2001). The 869 Jogan tsunami deposit and recurrence interval of large-scale tsunami on the Pacific Coast of northeast Japan. *Journal of Natural Disaster Science*, 23(2), 83–88.
- Monecke, K., Finger, W., Klarer, D., Kongko, W., McAdoo, B. G., Moore, A. L., & Sudrajat, S. U. (2008). A 1,000-year sediment record of tsunami recurrence in northern Sumatra. *Nature*, 455(7217), 1232–1234. <https://doi.org/10.1038/nature07374>
- Mortenson, M. C., Neilsen, T. B., Transtrum, M. K., & Knobles, D. P. (2023). Accurate broadband gradient estimates enable local sensitivity analysis of ocean acoustic models. *Journal of Theoretical and Computational Acoustics*, 31(2), 2250015. <https://doi.org/10.1142/S2591728522500153>
- Mousavi, S. M., & Beroza, G. C. (2023). Machine learning in earthquake seismology. *Annual Review of Earth and Planetary Sciences*, 51(1), 105–129. <https://doi.org/10.1146/annurev-earth-071822-100323>
- Musson, R. M. W. (2012). A provisional catalogue of historical earthquakes in Indonesia. *British Geological Survey*.
- Musson, R. M. W., & Jiménez, M. J. (2008). *Macroscopic estimation of earthquake parameters* (Vol. 3). NERIES project report, Module NA4, Deliverable D.
- Okada, Y. (1985). Surface deformation due to shear and tensile faults in a half-space. *Bulletin of the Seismological Society of America*, 75(4), 1135–1154. <https://doi.org/10.1785/bssa0750041135>
- Okal, E. A., & Reymond, D. (2003). The mechanism of great Banda Sea earthquake of 1 February 1938: Applying the method of preliminary determination of focal mechanism to a historical event. *Earth and Planetary Science Letters*, 216(1–2), 1–15. [https://doi.org/10.1016/S0012-821X\(03\)00475-8](https://doi.org/10.1016/S0012-821X(03)00475-8)
- Paskett, T., Whitehead, J., Harris, R., Ashcraft, C., Krometis, J., Sorensen, I., & Wonnacott, R. (2024). A tale of two faults: Statistical reconstruction of the 1820 Flores sea earthquake using tsunami observations alone. *Geophysical Journal International*, ggae044.
- Pranantyo, I. R., & Cummins, P. R. (2020). The 1674 Ambon tsunami: Extreme run-up caused by an earthquake-triggered landslide. *Pure and Applied Geophysics*, 177(3), 1639–1657. <https://doi.org/10.1007/s00024-019-02390-2>
- Reid, A. (2012). Historical evidence for major tsunamis in the Java subduction zone. *Asia Research Institute Working Paper Series*, 1–9.
- Reid, A. (2016). Two hitherto unknown Indonesian tsunamis of the seventeenth century: Probabilities and context. *Journal of Southeast Asian Studies*, 47(1), 88–108. <https://doi.org/10.1017/S002246341500048x>
- Reinwardt, C. G. C. (1858). Reis Naar het oostelijk gedeelte van den indischen archipel. In *Het Jaar 1821*.
- Ringer, H., Whitehead, J. P., Krometis, J., Harris, R. A., Glatt-Holtz, N., & Giddens, S. (2021). *Methodological reconstruction of historical seismic events from anecdotal accounts of destructive tsunamis: A case study for the great 1852 Banda arc mega-thrust earthquake and tsunami*. Journal of Geophysical Research. <https://doi.org/10.1029/2020JB021107>
- Sieh, K., Natawidjaja, D. H., Meltzner, A. J., Shen, C.-C., Cheng, H., Li, K.-S., et al. (2008). Earthquake supercycles inferred from sea-level changes recorded in the corals of West Sumatra. *Science*, 322(5908), 1674–1678. <https://doi.org/10.1126/science.1163589>
- Simanjuntak, A. V., & Ansari, K. (2023). Spatial time cluster analysis and earthquake mechanism for unknown active fault (kalatua fault) in the Flores sea. *Earth Science Informatics*, 16(3), 2649–2659. <https://doi.org/10.1007/s12145-023-01067-8>
- Singh, S. K., Astiz, L., & Havskov, J. (1981). Seismic gaps and recurrence periods of large earthquakes along the Mexican subduction zone: A reexamination. *Bulletin of the Seismological Society of America*, 71(3), 827–843. <https://doi.org/10.1785/bssa0710030827>
- Stein, S., Geller, R. J., & Liu, M. (2012). Why earthquake hazard maps often fail and what to do about it. *Tectonophysics*, 562, 1–25. <https://doi.org/10.1016/j.tecto.2012.06.047>
- Stuart, A. M. (2010). Inverse problems: A Bayesian perspective. *Acta Numerica*, 19, 451–559. <https://doi.org/10.1017/S0962492910000061>
- Sulaeman, H., Harris, R. A., Putra, P., Hall, S., Rafliana, I., & Prasetyadi, C. (2017). Megathrust earthquakes along the Java trench: Discovery of possible tsunami deposits in the Lesser Sunda Islands. *Geological Society of America Abstracts with Programs*, 49(6), 308722. <https://doi.org/10.1130/abs/2017AM-308722>
- Tanner, M. A., & Wong, W. H. (1987). The calculation of posterior distributions by data augmentation. *Journal of the American Statistical Association*, 82(398), 528–540. <https://doi.org/10.1080/01621459.1987.10478458>
- Tarantola, A. (2005). *Inverse problem theory and methods for model parameter estimation*. SIAM.
- UNISDR. (2009). Global assessment report on disaster risk reduction. *United Nations International Strategy for Disaster Reduction Secretariat*.
- Van Dyk, D. A., & Meng, X.-L. (2001). The art of data augmentation. *Journal of Computational & Graphical Statistics*, 10(1), 1–50. <https://doi.org/10.1198/10618600152418584>
- Wells, D. L., & Coppersmith, K. J. (1994). New empirical relationships among magnitude, rupture length, rupture width, rupture area, and surface displacement. *Bulletin of the Seismological Society of America*, 84(4), 974–1002. <https://doi.org/10.1785/bssa0840040974>
- Whitehead, J. P. (2025). *Tsunami methods: Jgr*. Zenodo. <https://doi.org/10.5281/zenodo.15889197>
- Wichmann, A. (1918). The earthquakes of the Indian archipelago to 1857. *Verhandl. Koninkl. Akad. van Wetenschappen*, 2nd sec, 20(4), 1–193.
- Wichmann, A. (1922). The earthquakes of the Indian archipelago from 1858 to 1877. *Verhandl. Koninkl. Akad. van Wetenschappen*, 2nd sec, 22(5), 1–209.
- Wonnacott, R., Stewart, D., Whitehead, J. P., & Harris, R. A. (2024). Methodological reconstruction of historical landslide tsunamis using Bayesian inference. *arXiv preprint arXiv:2404.14288*.
- Yu, S., & Ma, J. (2021). Deep learning for geophysics: Current and future trends. *Reviews of Geophysics*, 59(3), e2021RG000742. <https://doi.org/10.1029/2021rg000742>